ELSEVIER

Chemical Geology 175 (2001) 581–603

CHEMICAL GEOLOGY
INCLUDING
ISOTOPE GEOSCIENCE

www.elsevier.com/locate/chemgeo

Unusual bulk-rock compositions in eclogite-facies rocks from Syros and Tinos (Cyclades, Greece): implications for U–Pb zircon geochronology

Michael Bröcker [a,b,*], Michael Enders [a]

[a] *Institut für Mineralogie, Corrensstr. 24, D-48149 Münster, Germany*
[b] *Zentrallaboratorium für Geochronologie, Corrensstr. 24, D-48149 Münster, Germany*

Received 6 May 1999; accepted 28 July 2000

Abstract

Low-temperature eclogite-facies rocks from Syros and Tinos (Cyclades, Greece) include meta-ophiolitic blocks of unclear origin (meta-olistostrome or tectonic mélange). These blocks occur in a matrix of altered serpentinite and/or semipelitic to tuffitic schists. Some samples are characterized by very high trace-element concentrations, for example, eclogites from Tinos contain up to 4950 ppm Zr and up to 480 ppm Y. Understanding of the geochemical controls on the petrogenesis of these rocks has important consequences for interpretation of geochronological results. The emphasis of this study is on the behaviour of Zr under eclogite-facies P–T conditions. Due to remarkably high modal amounts of zircon, some samples from the meta-ophiolite suite are suitable for U–Pb zircon chronology. The geological significance of zircon ages can only be correctly interpreted by assessing whether zircon crystallized from a melt or formed during subsequent hydrothermal or metamorphic processes.

The results of this study lead us to conclude that infiltration of trace-element enriched fluids during eclogite-facies metamorphism caused local-scale compositional changes. Textural observations document the presence of a fracture network favouring fluid infiltration under high-pressure conditions. Such a system of microfractures might have provided infiltration paths for trace-element enriched fluids during earlier stages of high-pressure metamorphism. In most cases, subsequent recrystallization erased any evidence of the early infiltration channels, but inclusion of high-pressure phases in zircon provide evidence for this model, suggesting metasomatic alteration in a subduction-zone environment. The original fluid source and the conditions (e.g., high-F environment, highly saline brines?) under which commonly immobile elements were mobilized remain unclear. It is speculated that eclogitization of closely associated metagabbros may have released Zr and other trace elements. The results of this contribution suggest that new zircon formed during high-pressure metamorphism. Cretaceous U–Pb zircon ages are interpreted to date subduction metamorphism and not magmatic crystallization.

Keywords: Eclogites; Jadeitites; Syros; Tinos; Cyclades; Greece; Metasomatism; Trace-element enrichment; Rare earth elements

* Corresponding author. Institut für Mineralogie, Universität Münster, Corrensstr. 24, D-48149 Münster, Germany. Fax: +49-251-8338397.

E-mail addresses: brocker@nwz.uni-muenster.de (M. Bröcker), enders@nwz.uni-muenster.de (M. Enders).

0009-2541/01/$ - see front matter
PII: S0009-2541(00)00369-7

1. Introduction

High-pressure mélange sequences on the islands of Syros and Tinos (Cycladic blueschist belt; Fig. 1) comprise isolated blocks of meta-gabbros, eclogites, glaucophanites, jadeitites and serpentinites within a matrix consisting of serpentinitic or metasedimentary country rocks (Dixon and Ridley, 1987; Bröcker and Enders, 1999). There is a general consensus that the block–matrix association represents a disrupted meta-ophiolite, but it is not known whether blocks were included as metamorphic or magmatic rocks and whether all blocks have the same protolith or metamorphic ages. Different interpretations have been suggested to explain these occurrences and they include: a subduction-zone mélange (Altherr and Seidel, 1977); a shear zone that separates distinct thrust sheets (C. Ballhaus, pers. comm., 1998); a meta-olistostrome or meta-debris flow (Bonneau et al., 1980a,b; Hecht, 1984; Dixon and Ridley, 1987; Bröcker and Enders, 1999); erosion of a near-by ophiolitic nappe (Höpfer and Schumacher, 1997). It should be noted that these alternatives are not mutually exclusive: any lithostratigraphic horizon rich in serpentinized ultramafic rocks represents a zone of structural weakness that can easily develop into a

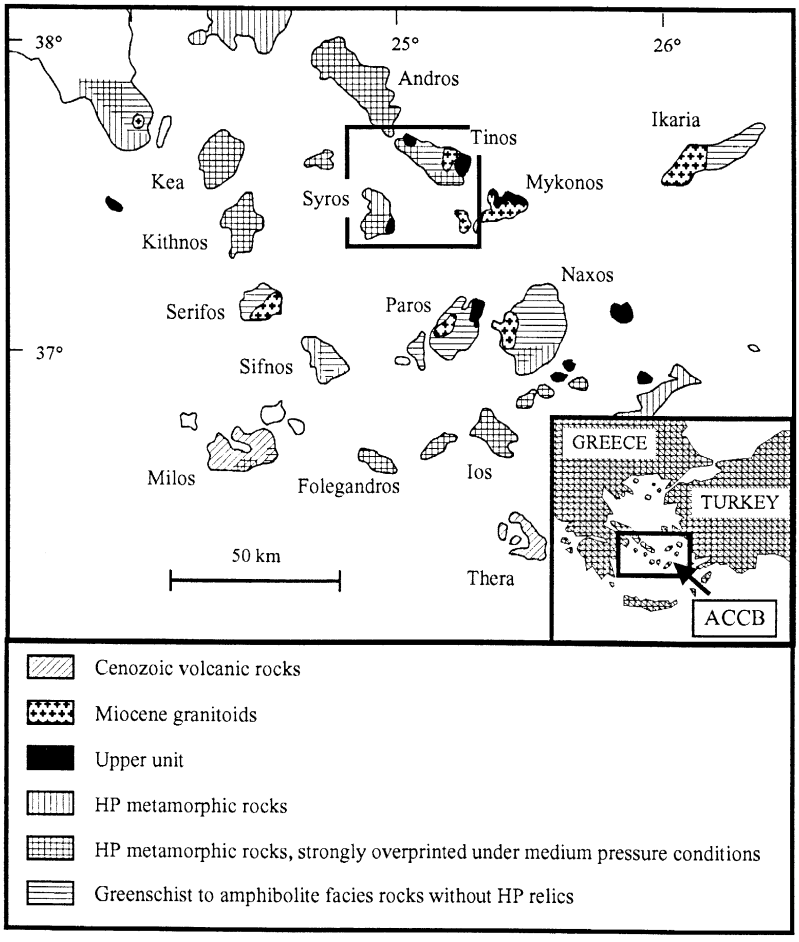

Fig. 1. Simplified geological map of the ACCB (after Altherr et al., 1982) indicating the regional distribution of the main metamorphic units and magmatic rocks.

shear zone. In the following, the term mélange is used in a non-genetic, descriptive sense.

Some mafic blocks display strong enrichment in elements commonly considered as relatively immobile (e.g., eclogites with Zr up to 4950 ppm; Y up to 480 ppm) and in rare earth elements (REEs) (up to 200 times chondritic values). The origin of the geochemical anomalies is controversial and was interpreted as related either to igneous (Seck et al., 1996) or to metasomatic processes (Dixon and Ridley, 1987; Bröcker and Enders, 1999). Dixon and Ridley (1987) attributed high concentrations of Ti, P and Na in the Syros mélange to compositional modifications caused by interaction with ultramafic rocks. Fluid-enhanced exchange processes between some blocks and the country matrix are recorded by reaction rinds (almost monomineralic glaucophane, sodic pyroxene, actinolite or chlorite; Dixon and Ridley, 1987). Metasomatic alteration is apparently not restricted to visible rinds as indicated by the common occurrence of Si-depleted rocks (SiO_2: 40.3–44.9 wt.%) within the groups of glaucophanites, eclogites, actinolitites and omphacitites (Kötz, 1989). This suggests widespread desilification as the result of the low SiO_2 activity in the serpentinite envelope (Dixon and Ridley, 1987). It seems conceivable that pervasive alteration also affected other elements. However, the extent of this metasomatism is unknown.

According to Seck et al. (1996), metasomatic alteration affected only a small percentage of mélange rocks. For most metabasic blocks, these authors considered isochemical metamorphism as more likely. TiO_2-rich (up to 9 wt.%) eclogites and garnet–glaucophanites were interpreted to be derived from ferrogabbroic protoliths, or from strongly differentiated basalts that crystallized in small-scale magma chambers. This interpretation was largely based on the observation that almost unmetamorphosed gabbroic rocks with similar Fe- and Ti-rich compositions were recognized elsewhere, e.g., in Eastern Liguria and the Northern Apennines. However, these authors also concluded that a fractional crystallization model alone fails to explain the compositional characteristics of the samples from Syros; the nature of a presumed contaminant remained unclear.

There is a large body of literature on meta-ophiolites suggesting that many compositional features recorded by their high-pressure derivatives are related to ocean floor alteration. These studies advocate the view that the subsequent eclogite-facies metamorphism is a largely isochemical process (e.g., Barnicoat and Cartwright, 1995, 1997; Scambelluri and Rampone, 1999). On the other hand, metasomatic modifications of ophiolitic precursors during subduction-zone metamorphism were also recognized in high-pressure mélange sequences, especially when isolated blocks are embodied inside an ultramafic matrix (e.g., Bebout and Barton, 1993; Sorensen and Grossman, 1993; Giaramita and Sorensen, 1994; Nelson, 1996). There is general consensus that parts of the Cycladic block–matrix associations were affected by post-magmatic alterations (Dixon and Ridley, 1987; Seck et al., 1996; Putlitz et al., 2000). However, the degree of chemical modifications and the timing of these processes is not completely understood; e.g., alterations caused by interaction between blocks and an ultramafic matrix, as indicated by reaction rinds, could be a multi-stage process with development of exchange rims at the ocean floor (Scambelluri and Rampone, 1999) and during high-pressure metamorphism. It is beyond the scope of this paper to evaluate the individual contributions of magmatic inheritance and distinct alterations (e.g., submarine weathering, low- and high-temperature alteration, interaction with ultramafic rocks, high-pressure metasomatism) that possibly have influenced all compositional features. However, the question whether unusual trace-element concentrations in some eclogites, omphacitites and jadeitites are mainly a primary feature of the protoliths, or the result of subsequent metasomatic modifications has important consequences for the interpretation of geochronological results. The emphasis is placed here on the behaviour of Zr. Enrichment in this element has caused notably high modal amounts of zircon, that make some blocks suitable for U–Pb chronology (Bröcker and Enders, 1999). The geological significance of zircon ages can only be correctly assessed if the processes controlling Zr mobility and zircon formation are understood, i.e., whether zircon crystallized from a melt or was newly formed during metamorphism, because of favorable Zr mobility amd supply. The results of this study lead us to conclude that metasomatic changes under eclogite-to-blueschist-facies conditions significantly contributed to Zr enrichment and that zircon chronol-

ogy dates an early episode of high-pressure metamorphism.

2. Geological setting

Syros and Tinos (Fig. 1) are part of the Attic–Cycladic Crystalline Belt (ACCB), which consists of two major structural groups of units, separated by low-angle faults (Dürr et al., 1978; Schliestedt et al., 1987; Okrusch and Bröcker, 1990). The upper group is rarely exposed and mainly consists of a heterogeneous sequence of unmetamorphosed Permian to Mesozoic sediments, ophiolites and Late Cretaceous greenschist-to-amphibolite-facies rocks. The lower group is the Cycladic blueschist unit that comprises a pre-Alpidic crystalline basement overlain by thrust sheets of a metamorphosed volcano-sedimentary sequence of Mesozoic age. The Cycladic blueschist unit has undergone two stages of Tertiary metamorphism. The first metamorphic event at eclogite-to-blueschist-facies conditions (T = c. 450–500°C, P = c. 15 ± 3 kbar; e.g., Okrusch et al., 1978; Matthews and Schliestedt, 1984; Bröcker et al., 1993) was caused by subduction of the Apulian microplate beneath the Eurasian continent (Bonneau, 1984). The second greenschist-to-amphibolite-facies metamorphism has been interpreted to result either from nearly isothermal decompression during uplift (northern Cyclades), or from renewed prograde metamorphism (southern Cyclades), reaching conditions of migmatization (e.g., Okrusch and Bröcker, 1990; Avigad et al., 1992). The high-pressure assemblages were widely overprinted by lower pressure counterparts, but relics of eclogites and blueschists still occur on many islands. Pressures attained during the main stages of overprint are estimated at 4 to 7 kbar (e.g., Avigad et al., 1992; Bröcker et al., 1993). K–Ar, Ar–Ar and Rb–Sr dating of white mica from blueschists and eclogites yielded Eocene ages between 53 and 40 Ma; white micas of greenschist- and amphibolite-facies assemblages provided ages between 25 and 18 Ma (e.g., Altherr et al., 1979, 1982; Wijbrans and McDougall, 1986, 1988; Maluski et al., 1987; Wijbrans et al., 1990; Bröcker et al., 1993). At present, attempts to date the high-pressure garnet–omphacite assemblages by means of the Sm–Nd method were unsuccessful, mainly because of mineral inclusions in garnet that lowered the Sm/Nd ratio with the result of unacceptable high uncertainties (Seck et al., 1996). A concordant U–Pb zircon age of 78 ± 1 Ma obtained for an omphacitite from Syros has been recently interpreted as related to a pre-Eocene high-pressure event (Bröcker and Enders, 1999). Detailed overviews of the geology and metamorphic evolution of the Cyclades are given by Dürr et al. (1978), Dürr (1986), Schliestedt et al. (1987) and Okrusch and Bröcker (1990).

2.1. Geology of Syros

Various aspects of field relationships, petrology, mineralogy and geochemistry were described by Dixon (1969), Ridley (1984), Ridley and Dixon (1984), Dixon and Ridley (1987), Kötz (1989) and Seck et al. (1996). Only a brief outline is summarized here.

Most part of Syros (Fig. 2) belongs to the Cycladic blueschist unit which occurs in two lithostratigraphic or tectonic subunits: (1) a volcano-sedimentary sequence (up to 2000 m in thickness), consisting of marbles, carbonate-bearing schists, metapelites, metabasic rocks, cherts and quartzites, that was affected by high-pressure metamorphism and a greenschist-facies overprint; (2) a structurally higher, meta-ophiolitic association which comprises isolated blocks of various high-pressure rock types in a matrix of altered serpentinites and/or semipelitic to tuffaceous schists (Bonneau et al., 1980a,b; Hecht, 1984; Dixon and Ridley, 1987). No difference in metamorphic grade was recognized between the lens-shaped to rounded tectonic blocks (meter to several tens of meters in size; Fig. 3a,b) and the matrix; they apparently shared the same deformation, eclogite-to-blueschist-facies recrystallization at identical P–T conditions and a subsequent greenschist-facies overprint. Genesis of this block–matrix sequence is unclear. It has been interpreted as a trench mélange, a metamorphosed olistostrome or as a tectonic shear zone (Altherr and Seidel, 1977; Bonneau et al., 1980a,b; Hecht, 1984; Dixon and Ridley, 1987; C. Ballhaus, pers. comm., 1998).

In southern Syros, two allochthonous units, both without any indications for high-pressure metamor-

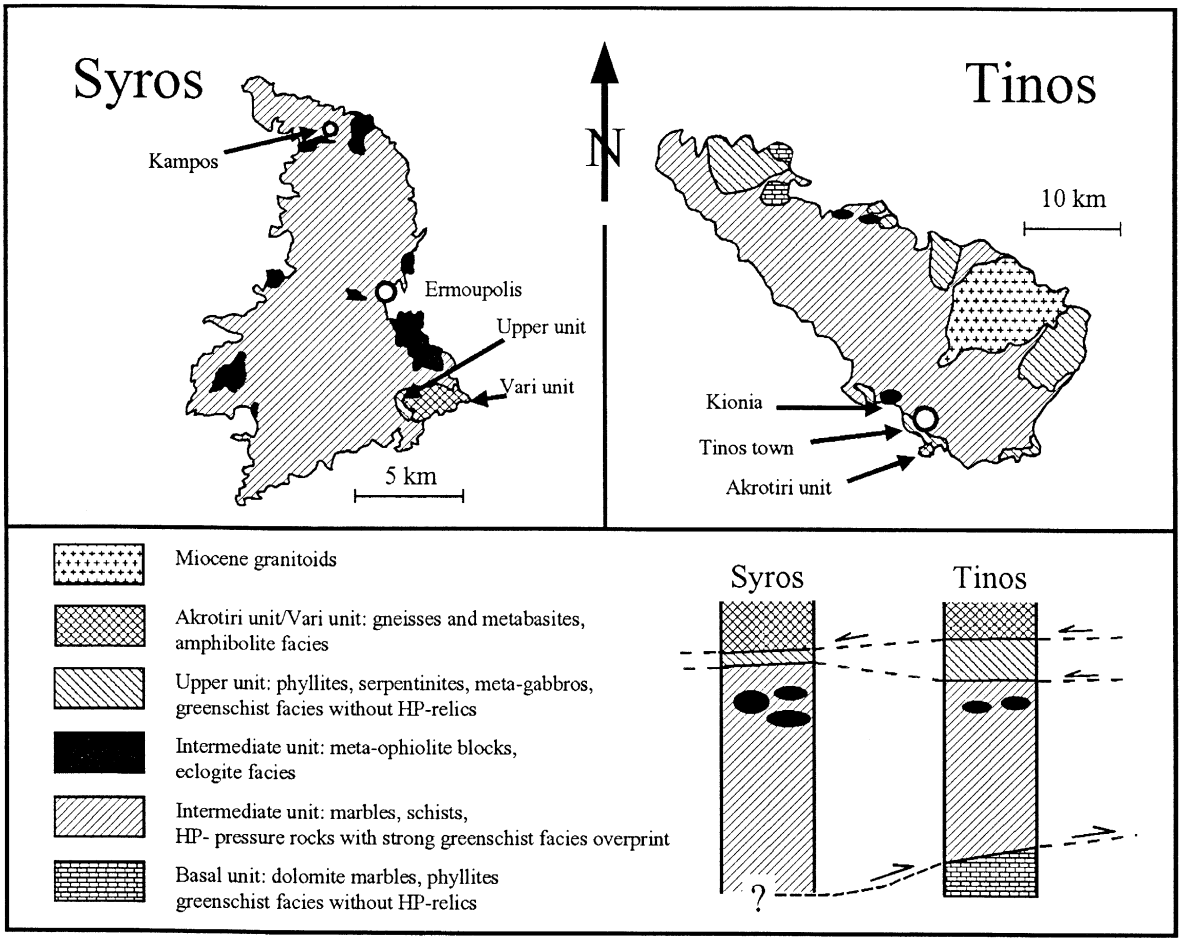

Fig. 2. Simplified geological maps of Syros (after Hecht, 1984; Ridley, 1984) and Tinos (after Melidonis, 1980 and Avigad and Garfunkel, 1989) indicating the sample locations discussed in the text. Schematic columnar sections (not to scale) indicate the major tectonic units.

phism, are found on top of the above-mentioned sequences (Fig. 2; Hecht, 1984; Ridley, 1984). For the uppermost amphibolite-facies rocks (Vari unit, Fig. 2), ^{40}Ar–^{39}Ar dating indicates Late Cretaceous metamorphism (c. 70 Ma; Maluski et al., 1987), as commonly observed in rocks of similar structural position in the Cyclades.

2.2. Geology of Tinos

On Tinos, four tectonic subunits can be distinguished (Fig. 2). The structurally highest Akrotiri Unit consists of amphibolite-facies rocks (Patzak et al., 1994). Amphiboles of metabasic layers yielded K–Ar dates between 77 and 66 Ma; muscovite from paragneisses provided K–Ar dates between 60 and 53 Ma (Patzak et al., 1994). The Akrotiri Unit is underlain by the Upper Unit, which consists of a disrupted meta-ophiolite sequence (up to about 250 m in thickness) affected by greenschist-facies metamorphism (Melidonis, 1980; Bröcker 1990a; Avigad and Garfunkel, 1989; Katzir et al., 1996; Stolz et al., 1997). Phyllitic rocks yielded Rb–Sr dates (phengite–whole rock) between 92 and 21 Ma that were interpreted to provide evidence for various and incomplete, deformation-related resetting of the Rb–Sr system during synmetamorphic tectonic stacking in

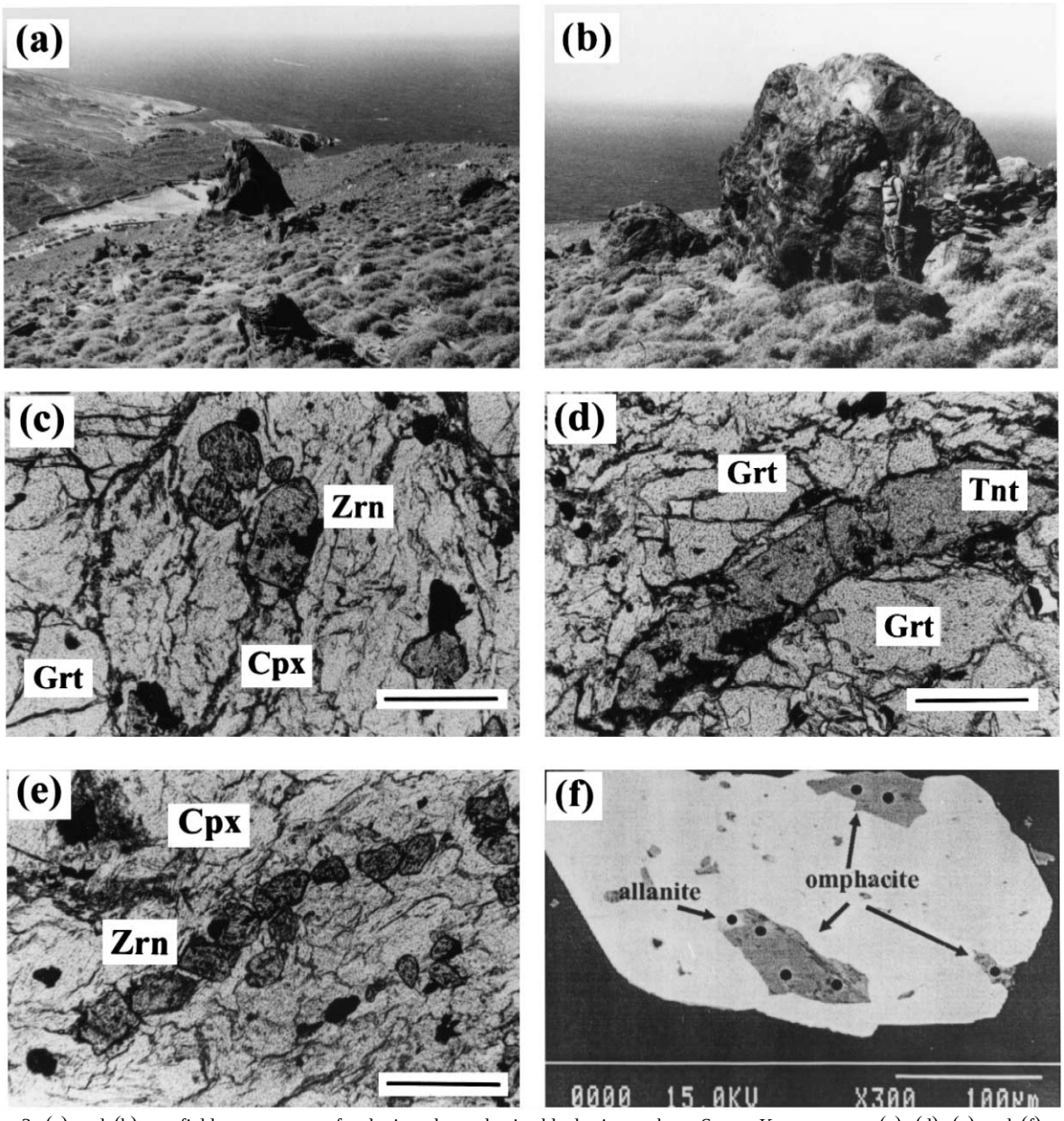

Fig. 3. (a) and (b) are field occurrences of eclogite–glaucophanite blocks in northern Syros, Kampos area; (c), (d), (e) and (f) are microphotographs of sample 1047: (c) zircon, in a matrix of omphacite and garnet in Zrn, length of scale = 310 μm; (d) titanite vein cross-cutting garnet, length of scale = 310 μm; (e) alignment of zircon in a matrix of omphacite, possibly mimicking a microfracture that acted as infiltration path for trace-element enriched fluids, length of scale = 310 μm; (f) back-scatter image of a zircon grain with inclusions of omphacite and allanite. Not labelled are small inclusions of rutile. Black dots indicate spots analysed with the electron microprobe.

the Oligocene (Bröcker and Franz, 1998). The Akrotiri and the Upper Units were not affected by high-pressure metamorphism and are considered equivalents of the allochthonous units that occur

above the blueschist-facies sequences on Syros (Fig. 2; Bröcker, in prep.).

The Cycladic blueschist unit is represented by a variegated sequence of marbles, calcschists, siliciclastic metasediments, cherts and basic and acidic metavolcanic rocks (up to about 1800 m in thickness; Melidonis, 1980), designated here as Intermediate Unit. Most rock types display greenschist-facies mineralogies, but remnants of eclogite- and blueschist-facies rocks are also preserved at many locations (e.g., Melidonis, 1980; Bröcker, 1990a).

The Basal Unit is only exposed in NW Tinos and consists mainly of various metamorphic carbonate rocks (Avigad and Garfunkel, 1989). Findings of undeformed fossils in dolomitic marbles (Melidonis, 1980), the absence of glaucophane and distinct deformational characteristics in phyllitic rocks were interpreted as evidence for significant metamorphic and microstructural differences compared to the overlying unit (Avigad and Garfunkel, 1989). The tectonic contact between the Intermediate and the Basal unit is a thrust fault (Avigad and Garfunkel, 1989); tectonic juxtaposition probably occurred during the Oligocene (Bröcker and Franz, 1998). In the eastern part of the island, the intrusion of Miocene granitoids caused contact metamorphism in parts of the Upper and Intermediate units (Avigad and Garfunkel, 1989; Altherr et al., 1982; Bröcker and Franz, 1994, 1998). For additional information on various aspects of the local geology, see Melidonis (1980), Avigad and Garfunkel (1989), Bröcker (1990a,b), Bröcker et al. (1993), Patzak et al. (1994), Katzir et al. (1996), Stolz et al. (1997), Bröcker and Franz (1994, 1998) and Bröcker and Enders (1999).

3. Analytical methods

3.1. Mineral analyses

Mineral compositions were determined with a SX-50 CAMECA microprobe at the Mineralogisches Institut, Universität Würzburg. Operating conditions were a 15-kV acceleration voltage, a 10-nA beam current and a counting time of 20–30 s. For standardization, natural and synthetic minerals were used. The raw data were corrected with a ZAF procedure using the PAP software provided by Cameca. Mineral assemblages of the studied samples are listed in Table 1. Selected electron microprobe analyses are reported in Tables 2 and 3.

Back-scattered electron (BSE) imaging was carried out on the JEOL microprobe at the Institut für Mineralogie, Universität Münster using an acceleration voltage of 15 to 20 kV and a beam current of 15 to 100 nA.

3.2. Bulk-rock analyses

Eleven samples were analyzed for major and selected trace elements with a Philips PW 2400 X-ray fluorescence (XRF) spectrometer at the Mineralogisch-Petrographisches Institut, Universität Köln. The REE Zr, Y, Nb, Hf, Ta, Th and U, were analysed by ICP-MS at Activation Laboratories, Ancaster, Ontario, using a lithium metaborate/lithium tetraborate fusion followed by acid digestion. For ICP-MS data, blank contributions were < 0.05 ppm. The very high concentrations of some high field strength elements (HFSE) are confirmed by the XRF results.

3.3. Isotope analyses

Isotope analyses were carried out at the Zentrallaboratorium für Geochronologie at the Institut für Mineralogie, Universität Münster using a VG Sector 54 multi-collector mass spectrometer (Sr, Sm, Nd) and a NBS-type Teledyne mass spectrometer (Rb). For Rb–Sr analyses, whole rock powders (about 100 mg) and mineral separates (c. 18–25 mg) were mixed with a ^{87}Rb–^{84}Sr spike in teflon screw-top vials and dissolved in a HF–HNO_3 (5:1) mixture on a hot plate overnight. After drying, 6 N HCl was added to the residue. This mixture was homogenized on a hot plate overnight. After a second evaporation to dryness, Rb and Sr were separated by standard ion-exchange procedures (AG 50W-X8 resin) on quartz glass columns using 2.5 and 6 N HCl as eluents. For mass-spectrometric analysis, Rb and Sr were loaded on Ta filaments with H_2O and H_3PO_4, respectively. Correction for mass fractionation is based on a $^{86}Sr/^{88}Sr$ ratio of 0.1194. Rb ratios were corrected for mass fractionation using a factor deduced from multiple measurements of Rb standard NBS 607.

Table 1
Mineral assemblages of eclogite-facies rocks from Syros and Tinos (Cyclades, Greece)

Sample	Location	Rock type	Cpx	Grt	Wm	Ep-I	Zrn	Tnt	Gln	Ab	Chl	Ep-II	Act	Others	Remarks
1045	Tinos	jadeitite	+	+	−	−	+	+	−	+G	+G	+G	+G	1, 2	7
1046	Tinos	eclogite	+	+	+	−	+	+	−	+G	+G	+G	−	1, 2	7
1047	Tinos	eclogite	+	+	−	−	+	+	+B	+G	+G	+G	+G	1, 2	7, 8
1049	Tinos	jadeitite	+	+	+	A	+	+	+B	+G	+G	+G	−	1, 2	7
1050	Tinos	jadeitite	+	+	+	+A	+	+	−	+G	−	+G	−	2	8
69	Tinos	omphacitite	+	−	+	−	−	+	−	+G	−	+G	−	−	8
412	Tinos	eclogite	+	+	+	+	−	+	+B	−	+G	−	+G	2, 3, 5	
564	Tinos	eclogite	+	+	+	−	−	+	+	−	+G	+G	−	2, 3	
702	Tinos	omphacitite	−	−	+	−	−	+	−	−	−	+G	−	−	
1079	Syros	blueschist	+	−	+	+	−	+	+	+G	−	−	−	2, 6	
1079	Syros	omphacitite	+	−	+	+	−	+	−	+G	−	−	−	2, 6	
1077	Syros	jadeitite	+	−	+	A	+	+	−	+G	+G	+G	−	−	
1078	Syros	jadeitite	+	−	+	−	+	+	−	+G	+G	+G	−	2	
1080	Syros	omphacitite	+	−	+	−	+	+	−	+G	−	+G	−	−	
1081	Syros	omphacitite	+	−	+	+A	+	+	−	−	+G	−	+G	1	7
1083	Syros	omphacitite	+	−	+	A	+	+	−	+G	+G	+G	−	4	
1085	Syros	omphacitite	+	−	+	+?	+	+	−	+G	+G	−	−	4	

+ Present; − not observed; G = related to the greenschist-facies overprint; B = related to the blueschist-facies overprint.
Mineral names: Cpx = clinopyroxene; Grt = garnet; Wm = white mica; Ep-I = first generation of epidote; A = allanite; Zrn = zircon; Tnt = titanite; Gln = glaucophane; Ab = albite; Chl = chlorite; Ep-II = second generation of epidote; Act = calcic amphibole.
Others: 1 = altered Ti-phase (ilmenite? rutile); 2 = opaques (mostly hematite); 3 = quartz; 4 = calcite; 5 = rutile; 6 = rutile rimmed by titanite.
Remarks: 7 = titanite is most likely a retrograde phase related to the blueschist-facies overprint; 8 = veins with cpx-II and/or titanite.

Total procedural blanks were less than 0.1 ng for Rb and 0.15 ng for Sr. Based on repeated measurements, the $^{87}Rb/^{86}Sr$ ratios were assigned an uncertainty of 1% (2σ). For other isotope ratios, uncertainties are reported at the $2\sigma_m$ level. Repeated runs of NBS standard 987 gave an average $^{87}Sr/^{86}Sr$ ratio of 0.710265 ± 24 (2σ, $n = 41$). All ages and elemental concentrations were calculated using the IUGS recommended decay constants (Steiger and Jäger, 1977). Rb–Sr ages were calculated using the least squares regression technique of York (1969). Ages and errors are reported at the 2σ level. The Rb–Sr isotopic data are summarized in (Tables 2, 3 and 5).

In order to ensure complete dissolution of zircon-rich whole rock powders, sample digestion for Sm–Nd studies was carried out in teflon bombs within screw-top steel containers, according to the method suggested by Krogh (1973) for zircon. In a first step, whole rock powders (c. 10–30 mg) were mixed with a $^{149}Sm/^{146}Nd$ spike in teflon screw-top vials and dissolved in a HF–HNO_3 (5:1) mixture on a hot plate overnight. The solution was then reduced to a small volume by evaporation on a hot-plate and transferred with fresh HF–HNO_3 (5:1) into teflon bombs. After a few days in steel autoclaves at 180°C, the dissolved samples were transferred to Savilex screw-top beakers. A few drops of $HClO_4$ were added to break down fluorides during drying on a hot-plate. After complete evaporation, 6 N HCl was added to the residue and excess HF and $HClO_4$ removed in a second evaporation step. Duplicates were analysed from a different aliquot of the powdered sample using the digestion technique for Rb–Sr samples and without adding $HClO_4$. Bulk REE were separated by standard ion-exchange procedures (AG 50W-X8 resin) on quartz glass columns using 2.5 and 6 N HCl as eluents. Sm and Nd were extracted from the REE fraction using teflon powder coated with 2-ethyl-hexyl phosphoric acid and 0.2 and 0.4 N HCl as elutant. For mass-spectrometric analysis, Sm and Nd were loaded with HCl on Re filaments using a triple filament configuration. Correction for mass fractionation is based on $^{142}Nd/^{144}Nd = 1.141862$, corresponding to $^{146}Nd/^{144}Nd$ ratio = 0.7219, as published by Patchett and Ruiz (1987). The $^{147}Sm/^{144}Nd$ ratios were assigned uncertainties

Table 2
Representative electron microprobe analyses of clinopyroxene from eclogite-facies rocks collected from Syros and Tinos

Sample	1047	1047	69	69	1045	1045	1049	1049	1081	1081	1083	1083	1085	1085	1077	1077
Spot	C8	C4	C1	B7	B1	B1	A2	A2	A2	A2	D1	D1	D2	D3	A2	X17
Type	matrix	vein	core matrix	vein	core matrix	rim matrix	core matrix	rim matrix	core matrix	rim matrix	core matrix	rim matrix	matrix	matrix	core matrix	matrix
SiO_2	55.76	53.35	53.93	53.04	56.84	56.83	57.67	57.85	54.99	54.68	55.43	55.16	56.37	56.69	58.68	58.26
TiO_2	0.12	0.12	0.04	0.06	0.19	0.12	0.00	0.06	0.11	0.08	0.07	0.09	0.08	0.11	0.06	0.06
Al_2O_3	12.99	7.34	9.52	3.74	16.71	16.76	19.90	20.63	11.30	9.93	10.09	9.91	10.60	11.79	22.02	20.86
Cr_2O_3	0.02	0.00	0.56	0.13	0.04	0.00	0.00	0.00	0.00	0.02	0.00	0.00	0.00	0.02	0.00	0.01
Fe_2O_3	5.49	14.57	5.67	7.18	5.04	4.73	2.80	2.40	9.18	8.74	4.97	6.09	2.80	2.54	0.44	1.65
MgO	5.68	3.86	8.40	9.89	2.14	2.27	1.36	1.33	5.87	6.73	6.40	6.48	8.25	7.52	1.54	1.58
CaO	9.10	8.22	14.13	18.88	3.70	3.90	2.38	2.41	9.85	10.96	10.52	10.62	12.93	11.29	2.26	2.44
MnO	0.06	0.20	0.31	0.49	0.10	0.10	0.03	0.01	0.14	0.19	0.13	0.20	0.17	0.14	0.05	0.08
FeO	1.21	3.57	0.90	3.94	3.10	3.05	2.78	2.94	0.80	1.56	3.87	3.06	2.04	1.91	2.70	1.66
Na_2O	9.43	9.21	6.52	3.71	12.16	12.05	13.09	13.11	9.00	8.10	8.06	8.11	7.32	8.19	13.33	13.37
K_2O	0.00	0.00	0.02	0.00	0.02	0.00	0.00	0.01	0.04	0.04	0.02	0.00	0.02	0.00	0.02	0.00
Total	99.87	100.44	99.99	101.08	100.03	99.81	100.01	100.76	101.28	101.03	99.57	99.71	100.56	100.19	101.11	99.98
Si	1.976	1.964	1.940	1.948	1.996	1.998	1.997	1.987	1.949	1.952	1.999	1.988	1.991	1.998	1.991	2.000
Ti	0.003	0.003	0.001	0.002	0.005	0.003	0.000	0.002	0.003	0.002	0.002	0.002	0.002	0.003	0.002	0.002
Al	0.542	0.318	0.404	0.162	0.691	0.694	0.812	0.835	0.472	0.418	0.429	0.421	0.441	0.490	0.881	0.844
Fe^{3+}	0.146	0.404	0.153	0.198	0.133	0.125	0.073	0.062	0.245	0.235	0.135	0.165	0.074	0.067	0.011	0.043
Cr	0.000	0.000	0.016	0.004	0.001	0.000	0.000	0.000	0.000	0.000	0.000	0.000	0.000	0.000	0.000	0.000
Mg	0.300	0.212	0.450	0.542	0.112	0.119	0.070	0.068	0.310	0.358	0.344	0.348	0.434	0.395	0.078	0.081
Ca	0.346	0.324	0.545	0.743	0.139	0.147	0.088	0.089	0.374	0.419	0.406	0.410	0.489	0.426	0.082	0.090
Mn	0.002	0.006	0.009	0.015	0.003	0.003	0.000	0.000	0.004	0.006	0.004	0.006	0.005	0.004	0.001	0.002
Fe^{2+}	0.036	0.110	0.027	0.121	0.091	0.090	0.080	0.084	0.024	0.047	0.117	0.092	0.060	0.056	0.077	0.048
Na	0.648	0.658	0.455	0.264	0.828	0.821	0.879	0.873	0.618	0.561	0.564	0.567	0.501	0.559	0.877	0.890
K	0.000	0.000	0.000	0.000	0.000	0.000	0.000	0.000	0.002	0.002	0.001	0.000	0.000	0.000	0.000	0.000
Total	4.000	4.000	4.000	4.000	4.000	4.000	4.000	4.000	4.000	4.000	4.000	4.000	4.000	4.000	4.000	4.000
Jadeite	52.2	28.8	34.4	11.0	71.1	71.5	83.6	85.5	42.4	37.8	44.1	41.9	43.6	49.5	90.9	86.1
Akmite	13.1	38.2	11.1	15.3	14.5	13.3	7.2	5.3	19.9	19.4	14.1	16.2	7.0	7.3	0.6	4.7
Augite	34.8	33.0	54.5	73.8	14.4	15.2	9.1	9.2	37.7	42.8	41.9	42.0	49.4	43.2	8.5	9.2

Structural formula on the basis of six oxygens and four cations. Fe^{3+} based on charge balance criteria.

Table 3
Representative electron microprobe analyses of white mica from eclogite-facies rocks collected from Syros and Tinos

Sample	1081	1081	1081	1081	1083	1083	1083	1083	1085	1085	1085	1085	1049	1049	1049	1049
Spot	A1	B1	C1	D1	A1	D1	E1	F3	B1	D2	F1	F2	B2	B4	E1	E2
SiO_2	49.04	50.30	50.24	48.76	48.87	49.22	49.25	49.44	51.31	49.85	50.03	50.06	46.76	46.82	46.80	47.22
TiO_2	0.17	0.17	0.19	0.22	0.29	0.25	0.39	0.32	0.15	0.20	0.19	0.16	0.08	0.07	0.00	0.06
Al_2O_3	27.42	27.61	25.99	28.23	28.28	28.26	28.96	28.98	27.75	29.62	28.28	28.19	38.91	39.08	39.48	39.88
Cr_2O_3	0.03	0.00	0.02	0.03	0.02	0.00	0.00	0.00	0.03	0.00	0.00	0.02	0.00	0.00	0.00	0.00
MgO	3.64	3.45	3.86	3.29	2.68	2.81	2.70	2.78	4.11	3.50	3.93	4.05	0.36	0.39	0.08	0.13
CaO	0.00	0.00	0.00	0.00	0.00	0.00	0.00	0.01	0.00	0.00	0.00	0.00	0.00	0.03	0.05	0.10
MnO	0.05	0.06	0.04	0.04	0.00	0.02	0.03	0.01	0.04	0.00	0.04	0.02	0.00	0.00	0.03	0.02
FeO	3.81	3.47	3.67	3.44	3.51	3.39	3.40	3.29	2.06	1.78	2.08	2.19	1.42	1.42	1.05	0.72
BaO	0.21	0.21	0.16	0.31	0.03	0.18	0.16	0.14	0.16	0.35	0.24	0.17	0.12	0.00	0.00	0.06
Na_2O	0.36	0.20	0.25	0.38	1.07	0.92	0.99	0.98	0.43	0.52	0.39	0.48	7.15	7.09	7.09	7.07
K_2O	10.73	10.86	10.74	10.55	9.53	9.79	9.54	9.54	10.26	9.87	10.20	10.35	1.01	0.95	0.84	0.85
H_2O	4.44	4.50	4.44	4.44	4.42	4.44	4.48	4.49	4.55	4.52	4.50	4.50	4.68	4.69	4.69	4.73
Total	99.91	100.82	99.60	99.68	98.70	99.29	99.89	99.97	100.84	100.20	99.87	100.20	100.49	100.53	100.11	100.84
Si	6.628	6.708	6.792	6.588	6.626	6.642	6.595	6.608	6.766	6.607	6.673	6.664	5.988	5.985	5.990	5.992
Ti	0.017	0.017	0.019	0.023	0.029	0.026	0.039	0.033	0.015	0.020	0.019	0.016	0.008	0.006	0.000	0.006
Al	4.368	4.340	4.141	4.495	4.520	4.495	4.571	4.565	4.312	4.626	4.445	4.424	5.874	5.888	5.955	5.964
Cr	0.003	0.000	0.002	0.003	0.002	0.000	0.000	0.000	0.003	0.000	0.000	0.003	0.000	0.000	0.000	0.000
Mg	0.733	0.685	0.778	0.662	0.541	0.565	0.539	0.553	0.808	0.691	0.780	0.803	0.068	0.074	0.016	0.025
Ca	0.000	0.000	0.000	0.000	0.000	0.000	0.000	0.002	0.000	0.000	0.000	0.000	0.001	0.004	0.007	0.014
Mn	0.006	0.007	0.004	0.005	0.000	0.002	0.003	0.001	0.004	0.000	0.005	0.002	0.000	0.000	0.003	0.002
Fe	0.431	0.387	0.414	0.389	0.398	0.383	0.381	0.368	0.227	0.198	0.232	0.244	0.152	0.152	0.112	0.076
Ba	0.011	0.011	0.008	0.016	0.002	0.009	0.008	0.007	0.008	0.018	0.013	0.009	0.006	0.000	0.000	0.003
Na	0.095	0.052	0.066	0.100	0.282	0.242	0.256	0.253	0.111	0.133	0.100	0.124	1.776	1.756	1.759	1.740
K	1.850	1.848	1.852	1.818	1.648	1.686	1.630	1.626	1.725	1.669	1.736	1.759	0.165	0.154	0.137	0.137
Total	14.142	14.055	14.077	14.099	14.048	14.049	14.023	14.016	13.980	13.962	14.003	14.048	14.038	14.019	13.980	13.958

Structural formula based on 22 oxygens.

of 0.3%. Uncertainties of the $^{143}Nd/^{144}Nd$ ratios are reported on the $2\sigma_m$ level. Repeated runs of the LaJolla standard gave an average $^{143}Nd/^{144}Nd$ ratio of 0.511847 ± 20 (2σ, $n = 13$).

Whole rock powders and phengite separates were prepared from small splits (< 1 kg) of larger samples (15–25 kg) collected for U–Pb studies. Samples were crushed in a jaw-crusher or steel mortar and an aliquot was ground in a tungsten carbide mill. For phengite separation, the remaining material was further reduced in size by grinding for a few seconds in a tungsten carbide mill. Following sieving fines were removed and mica was enriched by adherence to a sheet of paper. After hand-picking the mica packages under a stereomicroscope, possible contaminants located between invidual sheets were removed by grinding under ethanol in an agate mortar and pestle. Mica concentrates (optically pure $> 99\%$) were then washed in ethanol (p.a.) and H_2O (three times distilled) in an ultrasonic bath.

4. Sample locations and petrography

The investigated samples comprise omphacitites and jadeitites from Syros and eclogites, jadeitites and glaucophanites from Tinos (Table 1). Samples from Syros were collected in the Kampos area (Fig. 2), where the block–matrix association is exposed in a belt c. 3-km long and 1-km wide (Dixon, 1969; Dixon and Ridley, 1987). The meta-ophiolitic rocks occur as discrete blocks of variable size (up to several hundred meters) (Ridley and Dixon, 1984, Dixon and Ridley, 1987). In many cases, erosion has removed the serpentinitic or metasedimentary matrix of smaller blocks (< 10 m), which now occur as prominent boulders scattered throughout the northern belt (Fig. 3a,b).

Bröcker and Enders (1999) suggested that sporadic findings of blocks within the schist–marble sequence on Tinos are lithostratigraphic equivalents of the mélange on Syros. These occurrences include the meta-gabbro lens (several tens of meters in size) from the location Mavra Gremna (Melidonis, 1980) and several sites near Kionia which were sampled for this study (Fig. 2). Sample locations comprise (1) a coarse-grained glaucophanite–eclogite–omphacitite association (segregation banding?; samples 412, 414, 564) with obscure contacts to volcano-sedimentary country rocks, (2) a jadeitite block (up to several meters in diameter; samples 1049, 1050) enclosed in metasediments and (3) small, isolated eclogite and jadeitite blocks (samples 1045, 1046, 1047), which either represent discrete boulders (< 1 m) or fragments of the jadeitite outcrop (2). Smaller lenses may escape discovery due to intense ductile deformation and stretching. It is currently not known whether small boulders of omphacitites (usually < 30 cm) occurring elsewhere on the island represent boudinaged layers or incorporated blocks. On Tinos, blocks are not associated with an ultramafic matrix; reaction rinds were not observed.

4.1. Eclogites

At Tinos, eclogites occur in two modes: (a) as epidote-rich domains or layers (up to about 30 cm) within a large block of coarse-grained glaucophanite (samples 412, 564); (b) as isolated boulders (up to a about a meter in size; samples 1046, 1047) separated from the country rocks by erosion.

The mineral assemblage of the first type includes garnet ($Alm_{57-65}Prp_{6-10}Grs_{26-30}Sps_{2-3}$), omphacite, epidote, glaucophane, white mica, titanite, quartz and opaques. This assemblage possibly represents a transitional stage of the eclogite–blueschist transformation. Relics of igneous phases, corona textures or pseudomorphic replacement of igneous phases are not preserved and thus the protoliths cannot clearly be identified. The non-foliated, coarse-grained textures and locally preserved segregation banding suggests derivation from gabbroic precursors.

The second eclogite type (samples 1046, 1047) shows no indication of a blueschist-facies overprint and mainly consists of garnet ($Alm_{63-80}Prp_{4-20}Grs_{10-21}Sps_{1-5}$), omphacite (46–65 mol.% Jd, Fig. 4a), an altered Ti-phase and unusually high modal proportions of zircon (Fig. 3c,e). Zircon is apparently part of the high-pressure assemblage. About 50 to 80 zircon grains can be found in one thin-section (Bröcker and Enders, 1999), randomly distributed in the groundmass (Fig. 3c) and some as inclusions in garnet. Zircon was also found in linear arrays, re-

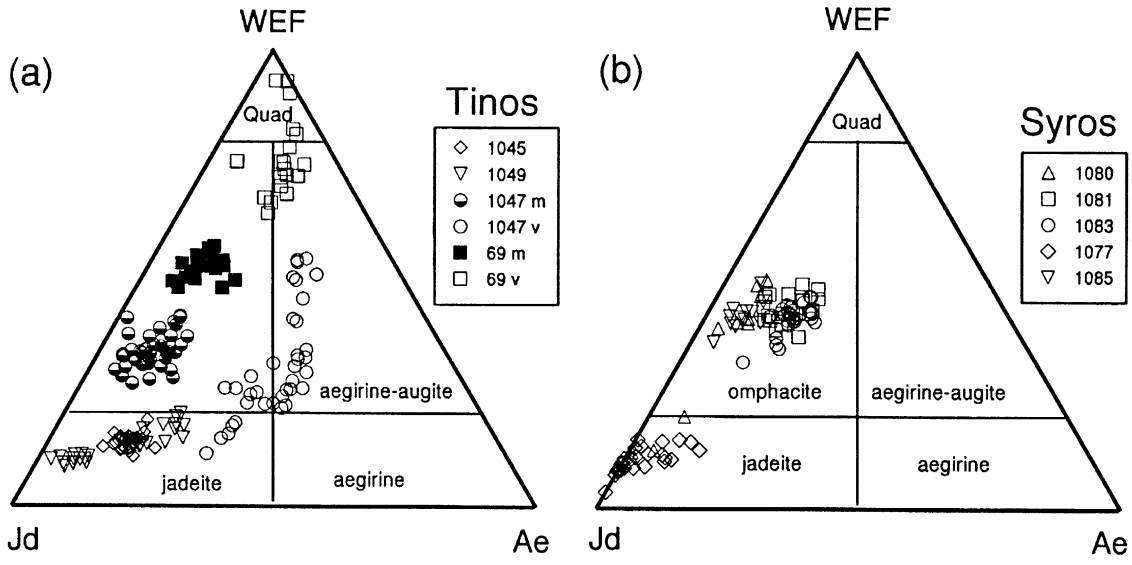

Fig. 4. Compositional variation of sodic clinopyroxene from (a) Tinos and (b) Syros; m = matrix; v = vein.

sembling microcracks, that cut the omphacite matrix, (Fig. 3e; cf. Fig. 3d). Inclusions of high-pressure phases in zircon document its formation during or after high-pressure metamorphism, due to favorable elemental supply (Fig. 3f). Zircon growth related to release of Zr by *retrograde* breakdown reactions in neighbouring rock volumes is considered unlikely, because zircon was not observed as a new phase in greenschist-facies veins or domains. Rather, fluid circulation under post-peak conditions is indicated by microfractures filled with clinopyroxene and titanite (Fig. 3d). These veins can be clearly distinguished from a later generation of microfractures with greenschist-facies assemblages, including chlorite, albite, epidote and calcic amphibole. Sodic pyroxene in veins (Fig. 4) has more variable jadeite contents (16–57 mol.%) than groundmass clinopyroxene and generally contains around 35 mol.% acmite component (28–43 mol.%).

The garnet–clinopyroxene thermometer (Ellis and Green, 1979), applied to the eclogite sample 1047, indicates temperatures of 610 ± 45°C (at 15 kbar), using compositions of garnet rims and clinopyroxene rims. The method of Krogh (1988) yielded a temperature of 514 ± 48°C (at 15 kbar). Temperatures were estimated assuming total Fe = Fe^{2+} and should only be considered as an upper limit. These results are in the range previously reported for high-pressure rocks from the Cyclades (Matthews and Schliestedt, 1984; Schliestedt, 1986; Bröcker et al., 1993; Höpfer et al., 1994).

In all studied samples, chlorite, albite, epidote-II and calcic amphiboles are typical secondary phases related to the greenschist-facies metamorphism. The blueschist- and greenschist-facies overprints require the influx of fluids: the limited volume extent of retrograde reactions suggests combination of rapid uplift and restricted fluid availability, either due to the absence of suitable infiltration paths or to insufficient influx of externally derived fluids.

4.2. Omphacitites

On Tinos (samples 69, 74, 702), omphacitites form thin layers (< 30 cm) or isolated lenses, but might have been more widespread. This is indicated by distinct geochemical characteristics of some greenschists (several meters in thickness), interpreted as retrograded omphacitites (Bröcker, 1991).

On Syros, omphacitites were found in two modes: (1) as small boulders within the meta-ophiolite association (samples 1080, 1081, 1083, 1085); (2) as

cm-scale layers interlayered with glaucophanites (sample 1079). Field observations suggest that the first type represents fragments of metasomatic reaction rinds (Dixon and Ridley, 1987; Bröcker and Enders, 1999). As on Tinos, it is unknown whether the second type indicates a primary interlayering derived from different magmatic protoliths, or is related to alteration processes.

The mineral assemblages of the various omphacitites (Table 1) mainly consist of sodic clinopyroxene (> 70 vol.%; 33–56 mol.% Jd; Fig. 4b), phengite (Si 6.5 to 6.8; Na/[Na + Ca + K] = 0.3–0.15), allanite-rich epidote, titanite and apatite. When present, garnet is a minor constituent. A small inclusion of uvarovite ($Uv_{74-84}Grs_{9-19}Alm_{3-4}Sps_2Adr_{<1}$) was recognized in sample 69. In all samples, chlorite and albite occur as secondary phases. It should be noted that most clinopyroxene of sample 1080 is omphacite, but small amounts of cpx found as inclusion in phengite are compositionally different with jadeite contents between 50 and 80 mol.%. In sample 69, monomineralic microfractures occur filled with cpx. This clinopyroxene contains 1–17 mol.% jadeite, 4–19 mol.% acmite and 67–93 mol.% augite (Fig. 4b).

4.3. Jadeitites

Jadeitites from Syros (samples 1077, 1078) are non-foliated, pale-green rocks that occur as volumetrically minor constituents of the meta-ophiolitic sequence. Commonly, actinolitic and/or chloritic blackwall zones or omphacite-rich zones rim individual jadeitite blocks. All samples show variable degrees of albitization. The primary mineral assemblage of the fine-grained samples comprises jadeite (> 80–90 vol.%; 80–90 mol.% jadeite component) and minor amounts of titanite, epidote, tremolitic amphibole and rare white mica. Albite and chlorite are typical secondary phases. Small amounts of retrograde analcime were identified in sample 1078. Nepheline was not recognized in the studied rocks. Conceivable precursors for jadeitites from Syros comprise plagiogranite and acidic metavolcanic rocks.

Jadeitites from Tinos (1045, 1048, 1049, 1050) are dark green in hand specimen and consist of jadeite (65–87 mol.% Jd, Fig. 4b), garnet ($Alm_{61-76}Prp_{5-18}Grs_{9-20}Sps_{2-7}$), paragonite (Na/[Na + Ca + K] = 0.89–0.95), allanite-rich epidote, an altered Ti-phase, zircon and apatite. The presence of epidote, chlorite, albite and calcic amphibole is related to the greenschist-facies overprint. Metasomatic reaction rinds along block margins were not recognized. The protoliths of jadeitites from Tinos cannot be reliably identified, but a derivation from a metasomatically altered, broadly basaltic precursor is likely.

5. Geochemistry

5.1. Major and trace elements

Major, minor and trace element concentrations of samples collected for this study are listed in Table 4. Whole rock data of samples 74, 412, 564, 702 were already reported by Bröcker (1991). All samples show complex bulk-rock compositions. Fig. 5 shows compositional variations of selected elements plotted against Mg-number (Mg# = 100 Mg/(Mg + Fe^{total}). MORB-normalized multi-element patterns are depicted in Fig. 6. In order to facilitate direct comparison with data presented by Seck et al. (1996), normalizing values for multi-element diagrams and REE abundances are those of Pearce (1983) and Evensen et al. (1978), respectively.

Bulk-rock compositions of eclogites (samples 1046, 1047) are broadly basaltic (SiO_2: 44.9–49.4 wt.%). Both samples are very rich in iron ($Fe_2O_3^{total}$: 14.7–19.4 wt.%). Mg-numbers are low (15–20); TiO_2 contents reach up to 2.8 wt.%. Concentrations of HFSE (e.g., Zr: 3383–4845 ppm; Y: 370–476 ppm; Nb: 66–87 ppm; Ce: 160–207 ppm; Nd: 120–163 ppm) are notably high. Cr (< 20 ppm) and Ni (< 33 ppm) contents are low.

Jadeitites range in SiO_2 from 54.9–61.9 wt.% and show very high Na_2O concentrations (10.5–11.9 wt.%). Samples from Tinos are characterized by lower SiO_2 (54.9–56.1 wt.%) and differ by considerably higher concentrations of $Fe_2O_3^{total}$ (8.9 to 10.0 wt.%) and MgO (2.0–2.3 wt.%) from samples collected on Syros ($Fe_2O_3^{total}$: 2.7–3.2 wt.%; MgO: 1.1–3.0 wt.%). Jadeitites from Tinos have Zr con-

Table 4
Whole rock compositions of eclogite-facies rocks from Syros and Tinos[a]

Sample	1045	1046	1047	1049	1050	1077	1078	1080	1081	1083	1085
SiO_2	54.91	49.39	44.88	54.86	56.05	61.91	60.18	54.55	51.75	53.13	53.02
TiO_2	0.97	1.47	2.78	1.25	1.03	0.74	0.48	0.71	1.98	1.04	0.27
Al_2O_3	16.83	15.73	15.74	17.18	16.4	19.58	17.72	17.2	13.34	15.74	21.38
Fe_2O_3	9.95	14.67	19.39	9.38	8.83	2.68	3.24	3.12	9.13	8.01	3.24
MnO	0.25	0.57	0.65	0.2	0.15	0.05	0.06	0.07	0.17	0.11	0.07
MgO	2.27	4.34	3.83	1.98	1.93	1.12	2.97	6.35	6.08	4.63	5.08
CaO	3.82	7.74	6.73	3.64	3.54	1.75	4.06	7.68	8.21	6.42	3.92
K_2O	0.01	0.09	0.03	0.04	0.3	0.05	0.17	3.63	1.55	2.84	5.94
Na_2O	10.72	6.05	4.56	10.67	10.98	11.89	10.45	5.22	6.67	6.44	4.05
P_2O_5	0.02	0.01	0.03	0.02	0.01	0.04	0.01	0.01	0.01	0.01	0.0
SO_3	0.04	0.04	0.05	0.02	0.03	0.02	0.01	0.01	0.02	0.02	0.01
L.O.I.	0.06	0.12	1.16	0.46	0.4	0.87	0.56	1.88	1.3	1.82	3.26
SUM	100.14	100.7	100.47	100.03	99.93	100.84	100.12	100.68	100.42	100.48	100.54
Mg#[b]	16.4	20.3	14.6	15.4	15.9	26.5	44.1	63.7	36.5	33.3	57.5
Sc	22	32	28	22	17	7	7	8	21	17	4
V	19	35	22	15	9	33	6	62	241	75	53
Cr	10	20	20	4	15	14	2	0	62	8	5
Ni	20	27	33	20	13	5	7	51	77	16	23
Rb	0.30	3.5	1.2	1	6.9	1	4.2	70.1	23.6	41.9	148.8
Sr	18.1	83.3	41.5	32	34.5	34.4	470.7	74.3	132.4	88	76.2
Y	159	371	478	242	71	67	92	52	95	90	96
Zr	1724	3483	4947	1985	2028	859	725	1076	627	1947	631
Nb	15	33	50	14	17	9.5	8.7	12	5.6	11	14
Ba	21	21	10	72	63	33	77	682	272	449	1471
Th	0.62	1.25	1.31	0.68	0.26	2.12	2.75	5.30	0.75	0.63	5.15
Hf	30.9	61.1	83.1	36.0	32.8	16.6	14.8	23.5	11.3	29.6	24.9
Ta[c]	*1.0*	*1.1*	*2.4*	*1.1*	*1.3*	*0.7*	*0.8*	*1.0*	*0.5*	*0.6*	*1.8*
U	0.5	1.5	1.1	0.6	0.3	1.0	1.0	2.2	0.6	0.7	1.9
La	21.3	41.2	62.1	24.1	10.3	14.8	33.8	15.2	10.2	20.2	26.1
Ce	69	134	198	77	33	39	85	44	29	61	72
Pr	11.7	22.4	31.4	12.6	5.70	5.67	11.8	6.25	4.60	9.86	10.1
Nd	63.3	121	167	69.9	31.4	27.1	54.0	27.5	24.0	50.0	44.8
Sm	18.0	34.4	46.9	19.7	8.72	6.47	12.8	6.32	7.20	13.0	11.6
Eu	5.755	11.86	15.75	6.780	3.071	2.331	3.103	2.013	8.591	5.900	3.919
Gd	20.8	41.8	54.9	20.9	10.1	7.78	13.9	6.34	9.71	13.9	12.8
Tb	4.08	7.99	11.1	3.73	1.75	1.42	2.52	1.08	1.96	2.34	2.49
Dy	25.5	52.5	73.3	22.8	10.9	9.21	15.2	6.66	13.1	14.1	15.0
Ho	5.53	12.4	16.3	4.84	2.51	2.12	3.19	1.59	3.03	3.03	3.13
Er	17.9	42.3	53.6	15.5	8.20	7.33	10.2	5.84	10.3	9.69	10.1
Tm	2.912	6.701	8.578	2.399	1.206	1.189	1.555	1.037	1.515	1.453	1.642
Yb	18.4	47.2	59.3	16.6	8.38	8.33	10.5	8.02	11.2	10.3	11.4
Lu	3.229	8.043	10.40	2.839	1.436	1.401	1.676	1.508	1.663	1.727	1.684
Eu_N/Eu_{N^*}	0.89	0.96	0.95	1.02	1.00	1.00	0.71	0.97	3.14	1.34	0.99
Zr/Hf	55.8	57.0	59.5	55.2	61.8	51.7	48.9	45.8	55.2	65.8	25.3

$Eu_N/Eu_{N^*} = Eu_N/\sqrt{(Sm_N \times Gd_N)}$.

[a]Analytical methods: Major elements and Sc, V, Cr, Ni by XRF; Rb and Sr by isotope dilution; Y, Zr, Nb, Ba, Th, Ta and rare earth elements by ICP-MS. Major elements in wt.%, trace elements in ppm.

[b]$Mg\# = 100\ Mg/(Mg + Fe^{2+})$.

[c]Due to sample preparation in a tungsten carbide mill, Ta concentrations are possibly not reliable.

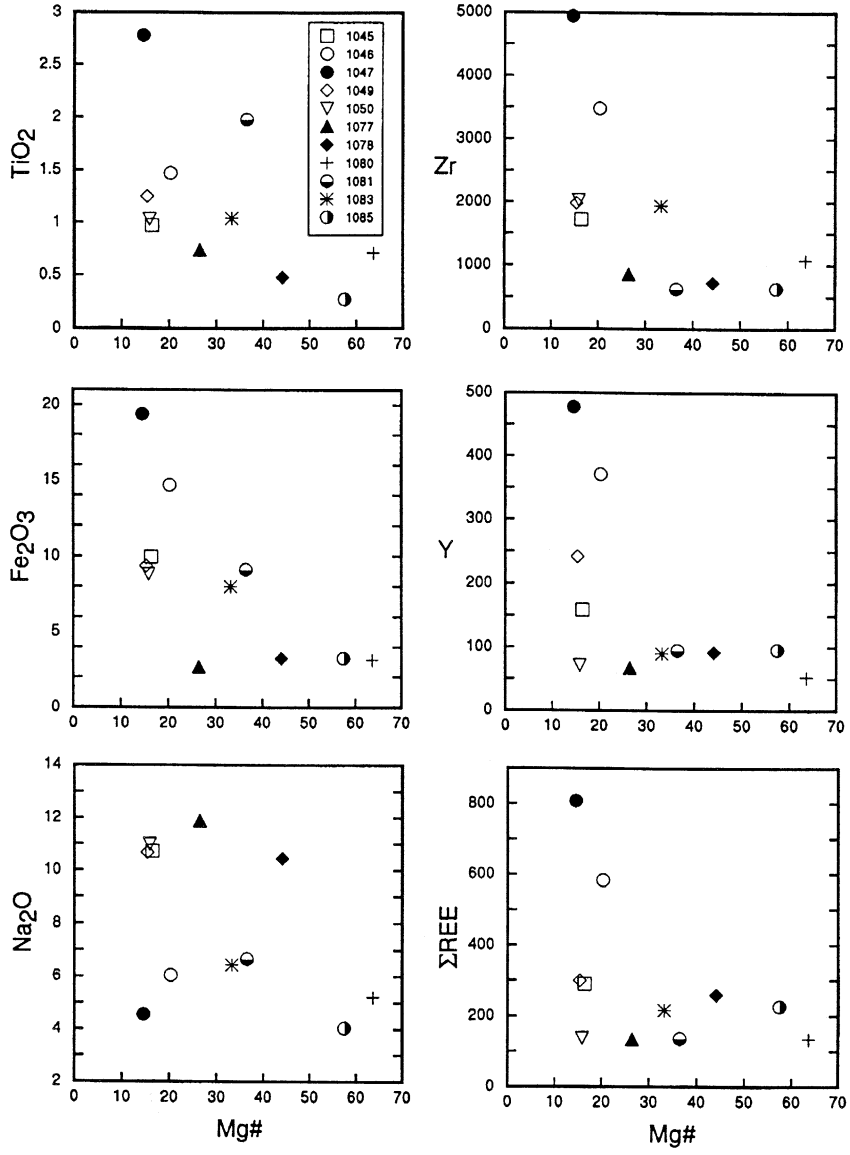

Fig. 5. Compositional variation of selected elements plotted against Mg#.

centrations ranging from 1594 to 1926 ppm. Samples from Syros contain 628–684 ppm of Zr. Omphacitites have basic compositions (SiO_2: 51.8–54.6 wt.%). K_2O (1.6–5.9 wt.%) concentrations are higher than in eclogites and jadeitites ($K_2O < 0.3$ wt.%). Zr contents range from 622 to 1592 ppm. In all rock types, P_2O_5 concentrations are very low (< 0.1 wt.%).

The MORB-normalized multi-element patterns have the same overall shape (Fig. 6). Spidergrams of eclogites and jadeitites (Fig. 6a) are characterized by considerable enrichment in high HFSE and marked troughs at P and Ti. Sr, K and Rb plot below or slightly above the MORB line. In the omphacitites K, Rb and Ba are enriched compared to the other samples. It should be noted that samples from a

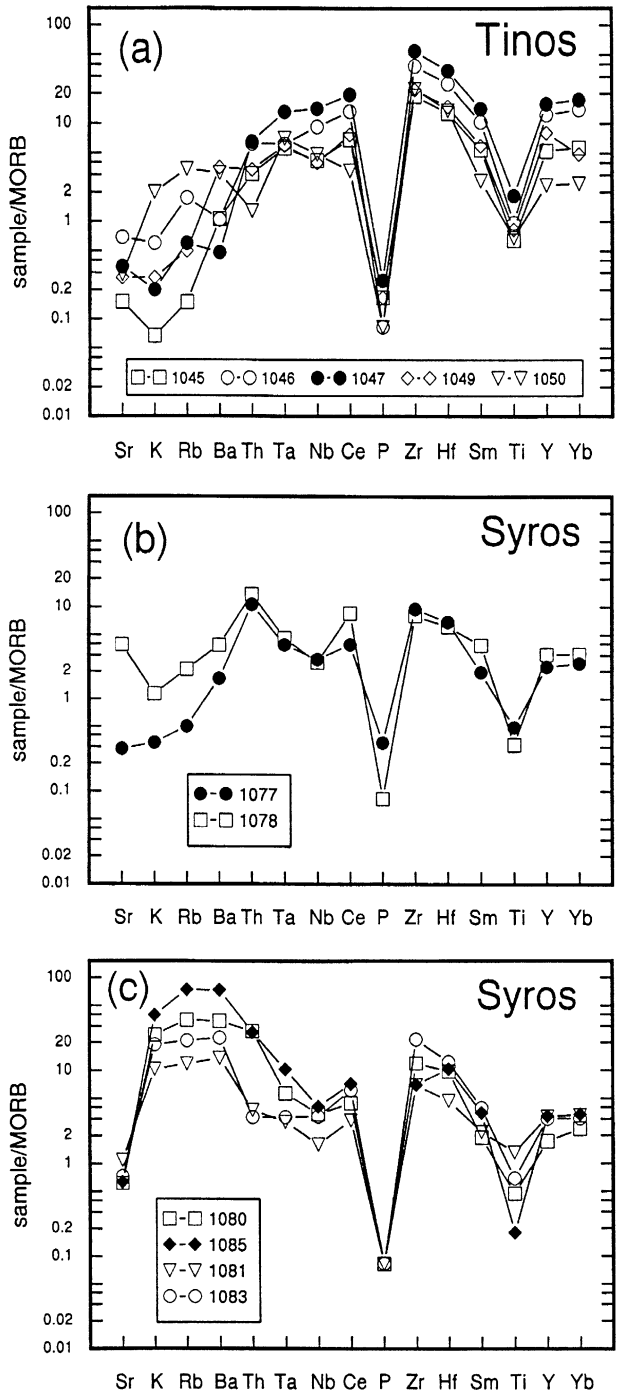

Fig. 6. MORB-normalized trace-element diagrams (after Pearce, 1983) for (a) eclogites and jadeitites from Tinos; (b) jadeitites from Syros and (c) omphacitites from Syros.

glaucophanite–eclogite block (412, 414, 564) and from omphacitites (74, 702) collected on Tinos do not show trace-element enrichment (Bröcker, 1991).

5.2. Rare earth elements

Four types of chondrite-normalized REE patterns can be distinguished. (1) Eclogites and jadeitites from Tinos show unusual sinusoidal REE variations with increase from La to Nd, then decrease towards Dy, followed by an increase to Lu. Pronounced Eu anomalies are absent ($Eu_N/Eu_{N^*} = 0.95–1.02$). Only sample 1045 displays a weak negative Eu anomaly (0.89). The overall shape of all patterns is similar but the degree of enrichment is variable (Fig. 7a). The highest ΣREE content is observed in the eclogites (150–208 times chondrite); the jadeitites are characterized by ΣREE abundances of 35–79 times chondrite. (2) Samples 1077 (jadeitite) and 1080 (omphacitite) from Syros display concave patterns with decreasing REE abundances towards Dy, followed by increasing ratios towards Lu. Both samples have no Eu anomaly (0.97–1.00). (3) Samples 1078 (jadeitite) and 1085 (omphacitite) from Syros show LREE-enriched patterns with $La_N/Yb_N = 2.2$ and 1.6 and $Eu_N/Eu_{N^*} = 0.71$ and 0.98, respectively. (4) The omphacitite 1081 is characterized by a continuously increasing pattern from La to Lu [$La_N/Yb_N = 0.62$] with a pronounced positive Eu anomaly ($Eu_N/Eu_{N^*} = 3.14$). Sample 1083 is more enriched in the LREE but has a similar pattern from La to Eu ($Eu_N/Eu_{N^*} = 1.32$) and from Ho to Lu. In contrast to sample 1081, REE abundances decrease from Sm to Ho.

None of these patterns shows similarities to REE abundances reported for various metabasic rocks from Syros (Kötz, 1989; Seck et al., 1996), Sifnos (Kötz, 1989; Mocek, 1994) and Tinos (Bröcker, unpubl. data). These workers reported either essentially flat patterns or variably LREE enriched, continuously decreasing REE abundances.

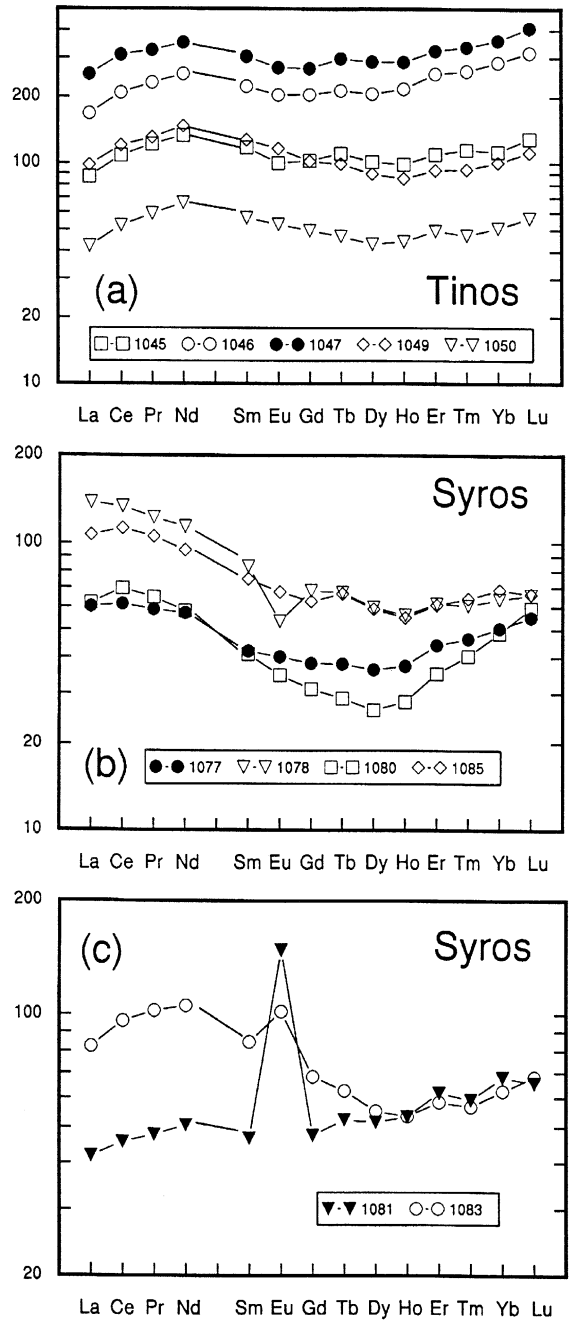

Fig. 7. Chondrite-normalized REE patterns (after Evensen et al., 1978) for (a) eclogites and jadeitites from Tinos; (b) and (c) jadeitites and omphacitites from Syros.

5.3. Rb–Sr and Sm–Nd isotope results

Rb–Sr and Sm–Nd data are listed in Tables 5 and 6. Measured Sr isotope compositions range from $^{87}Sr/^{86}Sr = 0.70468–0.70908$. $^{87}Rb/^{86}Sr$ ratios range from 0.01 to 5.66, but mostly are below 0.6

Table 5
Rb–Sr isotopic results of high-pressure rocks from Syros and Tinos

Sample	Type	Rb (ppm)	Sr (ppm)	$^{87}Rb/^{86}Sr$[a]	$^{87}Sr/^{86}Sr$	$^{87}Sr/^{86}Sr_{(80)}$	$^{87}Sr/^{86}Sr_{(200)}$
1045	whole rock	0.288	18.06	0.0461	0.705092 (24)[b]	0.705039	0.704961
1045[c]	whole rock	0.289	17.58	0.0475	0.705064 (22)	0.705010	0.704929
1046	whole rock	3.533	83.28	0.123	0.704939 (20)	0.704800	0.704590
1047	whole rock	1.200	41.54	0.0835	0.704909 (19)	0.704814	0.704671
1048	whole rock	0.236	10.74	0.0636	0.704678 (57)	0.704606	0.704497
1049	whole rock	0.960	31.99	0.0869	0.706051 (24)	0.705952	0.705804
1049[c]	whole rock	0.976	31.91	0.0885	0.706014 (26)	0.705914	0.705763
1050	whole rock	6.891	34.60	0.576	0.706431 (24)	0.705776	0.704793
1050[c]	whole rock	6.942	34.54	0.581	0.706419 (22)	0.705758	0.704765
1077	whole rock	0.952	34.35	0.0802	0.705931 (18)	0.705840	0.705703
1078	whole rock	4.225	470.7	0.0260	0.705928 (25)	0.705899	0.705854
1080	whole rock	70.12	74.28	2.73	0.707147 (23)	0.704043	*(0.699380)*[d]
1081	whole rock	23.62	132.4	0.516	0.705121 (20)	0.704534	0.703653
1081[c]	whole rock	23.23	130.9	0.513	0.705163 (23)	0.704579	0.703703
1081	phengite	141.0	67.25	6.07	0.709062 (29)		
1083	whole rock	41.86	87.96	1.38	0.706084 (21)	0.704519	0.702168
1083	phengite	130.8	59.18	6.40	0.709390 (18)		
1085	whole rock	148.82	76.15	5.67	0.709081 (20)	0.702654	*(0.692999)*[d]
414	whole rock	1.560	147.7	0.0306	0.705276 (16)	0.705241	0.705189
412	whole rock	2.062	122.0	0.0489	0.705570 (21)	0.705514	0.705431
564	whole rock .	4.680	142.2	0.0952	0.706042 (19)	0.705934	0.705771
702	whole rock	51.86	152.9	0.981	0.705829 (19)	0.704713	0.703038
74	whole rock	0.797	306.8	0.00751	0.706732 (23)	0.706724	0.706711

[a] Based on repeated measurements, the $^{87}Rb/^{86}Sr$ ratios were assigned an uncertainty of 1%.
[b] Numbers in parentheses indicate uncertainties in ratios (last two digits) quoted at the 2 σ_m level.
[c] Duplicate analysed from a different aliquot of the same whole rock powder.
[d] This unrealistic low value is caused by uncertainties resulting from the high $^{87}Rb/^{86}Sr$ ratios.

Table 6
Sm–Nd isotopic results of high-pressure rocks from Syros and Tinos

Sample	Sm (ppm)	Nd (ppm)	$^{147}Sm/^{144}Nd$[a]	$^{143}Nd/^{144}Nd$[b]	εNd_0	$^{143}Nd/^{144}Nd_{80}$	εNd_{80}	$^{143}Nd/^{144}Nd_{200}$	εNd_{200}
1045	17.70	60.99	0.1755	0.513029 (15)	7.6	0.51294	7.8	0.51280	8.2
1046	33.17	114.81	0.1747	0.513042 (15)	7.9	0.51295	8.1	0.51281	8.4
1046[c]	32.82	114.07	0.1739	0.513015 (14)	7.4	0.51292	7.6	0.51279	7.9
1047	46.48	164.56	0.1708	0.513009 (17)	7.2	0.51292	7.5	0.51279	7.9
1047[c]	46.41	164.52	0.1705	0.512984 (17)	6.7	0.51289	7.0	0.51276	7.4
1048	16.46	57.65	0.1726	0.513025 (17)	7.5	0.51293	7.8	0.51280	8.2
1049	18.21	61.91	0.1778	0.512973 (33)	6.5	0.51288	6.7	0.51274	7.0
1050	8.53	30.01	0.1718	0.513015 (24)	7.4	0.51293	7.6	0.51279	8.0
1077	6.65	27.40	0.1467	0.513030 (19)	7.6	0.51295	8.2	0.51284	8.9
1078	13.76	59.24	0.1404	0.512996 (20)	7.0	0.51292	7.6	0.51281	8.4
1080	6.60	29.13	0.1369	0.513000 (18)	7.1	0.51293	7.7	0.51282	8.6
1081	6.57	21.40	0.1856	0.513011 (17)	7.3	0.51291	7.4	0.51277	7.6
1083	11.06	41.41	0.1615	0.512993 (26)	6.9	0.51291	7.3	0.51278	7.8
1085	11.48	44.58	0.1558	0.513029 (20)	7.6	0.51295	8.0	0.51283	8.7

[a] Based on repeated measurements, the $^{147}Sm/^{144}Nd$ ratios were assigned an uncertainty of 0.3%.
[b] Numbers in parentheses indicate uncertainties in ratios (last two digits) quoted at the $2\sigma_m$ level.
[c] Duplicate made from a different aliquot of the same whole rock powder using a different digestion technique. For details see Analytical methods.

and thus require very little correction for in situ ^{87}Rb decay. Measured Nd isotope compositions vary between $^{143}Nd/^{144}Nd = 0.51298–0.51304$. The spread in $^{147}Sm/^{144}Nd$ ratios is small (0.1369–0.1856). Recalculated initial $^{87}Sr/^{86}Sr$ and εNd values calculated for 200 Ma (inferred protolith age, not constrained by geochronology or paleontological data from associated metasediments) and 80 Ma (timing of high-pressure metamorphism; Bröcker and Enders, 1999) define a small range in isotope compositions (Tables 5 and 6). The Sr–Nd isotope characteristics provide no indication for derivation or involvement of sources originating in the continental crust. Rb–Sr phengite–whole rock dating of two omphacitites (samples 1081, 1083) provided ages of 49.4 ± 0.7 and 46.3 ± 0.7 Ma (Fig. 8; Table 5) that are in the range obtained by previous white mica dating using the $^{40}Ar–^{39}Ar$ technique (Maluski et al., 1987; Baldwin, 1996).

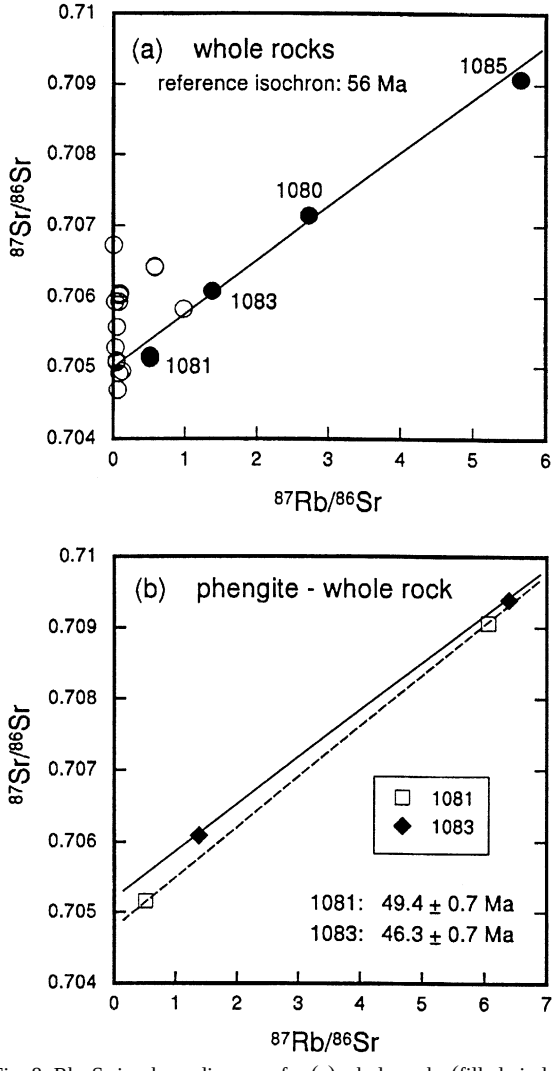

Fig. 8. Rb–Sr isochron diagrams for (a) whole rocks (filled circles indicate samples used for reference isochron) and (b) phengite–whole rock pairs used for geochronology; see text for details.

6. Discussion

A small percentage of mélange rocks from Syros and Tinos is characterized by remarkable trace-element enrichments. This compositional feature is absent in the coherent high-pressure units of the Cycladic blueschist belt (e.g., Bröcker 1990b; Mocek, 1994). A suitable monitor for trace-element enrichment in the mélange blocks is a high modal proportion of zircon (Bröcker and Enders, 1999). A major problem concerns the origin of this enrichment and its bearing on the significance of U–Pb zircon ages. Petrographic evidence clearly suggests Zr-mobility at high-pressure conditions (Fig. 3f). The question arises, whether the Zr is mobilized from within the samples (closed system redistribution) or is incoming from external sources, either as the result of local-scale mobility, or due to extensive fluid influx. Although Zr is commonly considered as a relatively immobile element, its mobility has been recognized in a wide range of geological environments, including hydrothermal and metamorphic settings (e.g., Rubin et al., 1989, 1993; Gieré, 1990; Pan and Fleet, 1996; Fraser et al., 1997). In such cases, metasomatic fluids also mobilized other HFSE (Ti, Th, Nb, Y) and REEs (e.g., Rubin et al., 1989, 1993; Gieré, 1990). Important agents for the transport are fluorine- and chlorine-bearing aqueous fluids; PO_4^{3}, SO_4^{2-}, and CO_3^{2-} were also suggested as ligands for complexing (Rubin et al., 1989, 1993; Pan and Fleet, 1996; Fraser et al., 1997).

Based on the study of mélange sequences from Washington and California, Sorensen and Grossman (1993, p. 295) concluded that "*mobilization of incompatible elements in fluids and deposition of such elements in the accessory phases of mafic and ultramafic rocks appears to result from certain P–T-fluid*

conditions in subduction zones". Direct evidence for mobility and transport of HFSE and light REE was provided by a fluid inclusion study of eclogites from the Monviso Complex, Italian Western Alps (Philippot and Selverstone, 1991). Identification of different silicate, oxide and carbonate daughter crystals (e.g., baddeleyite, monazite, rutile, titanite) in aqueous brines demonstrated increased solubilities and local scale mobility for many trace elements under high-pressure conditions (Philippot and Selverstone, 1991; Nadeau et al., 1993). Moderate salinities in early aqueous fluids were also reported for blueschist-facies rocks from Syros (Barr, 1990), suggesting favourable circumstances for trace-element mobilization. Millimeter-scale veins with late high-pressure assemblages (almost monomineralic sodic clinopyroxene or titanite) were observed in several samples from Tinos. We assume that such a network of microfractures, induced by cataclastic deformation of rigid blocks in a ductile deforming matrix, provided infiltration paths for trace-element enriched fluids during earlier stages of high-pressure metamorphism. The original infiltration channels were mostly erased by subsequent recrystallization, but mimetic replacements of veinlets are sporadically preserved (Fig. 3e). This interpretation is supported by Zr/Hf ratios. Natural igneous rocks are characterized by values close to the C1-chondritic ratio of 38 (e.g., Bau, 1996). In contrast, Zr and Hf are strongly fractionated in aqueous media. Thus, the non-chondritic Zr/Hf values of the relevant samples (Table 4) are in agreement with a model suggesting fluid-mediated redistribution processes.

The source of the Zr remains unclear, but we suggest that the enrichment is genetically linked to the eclogitization of the meta-gabbros which form the dominant rock type of the block–matrix associations. Mafic igneous minerals could contain relatively high Zr concentrations, whereas major high-pressure minerals (Na-pyroxene and garnet) commonly have negligible Zr contents (e.g., Messiga et al., 1995). Trace-element compositions of clinopyroxenes from blueschist and eclogitized Fe–Ti gabbros from the Ligurian Alps indicate that, relative to original igneous diopside, the high-pressure clinopyroxenes are markedly depleted in Zr, Y, and Ti (Messiga et al., 1995). Uptake of these elements by zircon, Ti-minerals or other phases may result in a closed-system redistribution within the original protolith. However, if fluids of suitable compositions are present, migration of solutes into neighbouring rock-volumes seems to be a viable mechanism to explain metasomatic alteration of closely associated rocks. This also raises the question to what extent the TiO_2 concentrations of mélange rocks (e.g., 3–9 wt.% in eclogites and glaucophanites from Syros; Kötz, 1989; Seck et al., 1996) are actually inherited from the magmatic precursors. Redistribution of Ti, as indicated by rutile or Ti-clinohumite crystallization in eclogite-facies veins that contain high-salinity fluid inclusions is commonly observed in high-pressure terrains (Philippot and Selverstone, 1991; Scambelluri et al., 1997, 1998). In the studied samples, petrographic evidence indicates that Zr was mobilized and redistributed during the high-pressure event. It is unlikely that only Zr was affected by this process. If available, other elements with similar geochemical properties will show coherent behaviour. Thus, redistribution of Ti, Y and the REE is a reasonable concept. Mobilization of Ti is clearly documented by monomineralic titanite veins (Fig. 3c), suggesting that HFSE were soluble in synmetamorphic fluids. As a consequence, the assumption that the TiO_2 concentrations of the mélange rocks are unaltered compositional features inherited from the magmatic protoliths is not necessarily valid. The derivation of Ti-rich eclogites and glaucophanites from highly evolved magmatic liquids, as suggested by Seck et al. (1996), is not unambiguously demonstrated.

Whatever the interpretation, our textural and chemical analysis indicates that Zr was mobilized in the eclogitic fluids and migrated at variable distances from the source, being involved in a fluid-mediated redistribution process. The effectiveness of Zr redistribution in the high-pressure fluids and zircon recrystallization during eclogite-facies conditions is further indicated by the observation that the studied zircons do not show distinctive inherited cores overgrown by metamorphic rims.

7. Summary and conclusions

In the Cyclades, high-pressure/low-temperature rocks mostly occur in structurally coherent se-

quences. On the islands of Syros and Tinos, a block–matrix association was recognized: it consists of isolated boulders of meta-gabbros, eclogites, glaucophanites, omphacitites, jadeitites and ultramafic rocks, that are associated with a matrix of altered serpentinite or metasediments (Bonneau et al., 1980a,b; Hecht, 1984; Dixon and Ridley, 1987; Bröcker and Enders, 1999). A small percentage of mélange rocks is characterized by unusual bulk-compositions with remarkable enrichment in HFSEs and/or the REEs. It is suggested here that metasomatic changes, which likely occurred under eclogite-to-blueschist-facies conditions, significantly contributed to the generation of this compositional feature. High modal proportions of zircon are considered to be a monitor for subduction-related metasomatism. This argument is strengthened by petrographic evidence. Inclusions of high-pressure minerals in zircon suggest that new zircon grew during high-pressure metamorphism, as a result of favorable elemental supply. The original source and the conditions (e.g., high-F environment, highly saline brines?) under which commonly immobile elements were mobilized remain unclear. However, it is speculated that eclogitization of metagabbros may have released Zr and other trace elements. Focused infiltration along a network of microfractures metasomatically altered small rock volumes. Subsequent recrystallization erased any evidence of the early infiltration channels but inclusions of high-pressure phases in zircon provide important constraints on the timing of this process. Favorable conditions for trace-element mobilization and re-precipitation apparently were restricted to relatively small domains within the subduction complex (cf. Philippot and Selverstone, 1991; Selverstone et al., 1992).

The interpretation presented here has significant implications for the understanding of geochronological results from the Cyclades. Many blocks from the mélange are suitable for U–Pb zircon chronology. For samples from Syros, in-situ SHRIMP and conventional U–Pb multi-grain dating yielded zircon ages of c. 75–78 Ma (Keay, 1998; Bröcker and Enders, 1999). The results of this contribution suggest that these ages provide constraints for the timing of high-pressure metamorphism, establishing evidence for a Cretaceous subduction environment in the Cyclades.

Acknowledgements

Thanks are due to H. Baier for laboratory assistance and to S. Rochnowski for support on the mass spectrometer. Discussions with C. Ballhaus and K. Mezger contributed significantly to this work. We thank M. Scambelluri, R. Tribuzio and M. Thöni for careful reviews and helpful suggestions that greatly improved the quality of this paper. Financial support of the Deutsche Forschungsgemeinschaft (Br 1068/3-1) is greatly acknowledged.

References

Altherr, R., Seidel, E., 1977. Speculations on the geodynamic evolution of the Attic–Cycladic crystalline complex during alpidic times. Proc. Colloq. Geol. Aegean Reg., 6th 1, 347–352.

Altherr, R., Schliestedt, M., Okrusch, M., Seidel, E., Kreuzer, H., Harre, W., Lenz, H., Wendt, I., Wagner, G.A., 1979. Geochronology of high-pressure rocks on Sifnos (Cyclades, Greece). Contrib. Mineral. Petrol. 70, 245–255.

Altherr, R., Kreuzer, H., Wendt, I., Lenz, H., Wagner, G.A., Keller, J., Harre, W., Höhndorf, A., 1982. A Late Oligocene/Early Miocene high temperature belt in the Attic–Cycladic Crystalline Complex (SE Pelagonian, Greece). Geol. Jahrb., Reihe E 23, 97–164.

Avigad, D., Garfunkel, Z., 1989. Low angle faults underneath and above a blueschist belt — Tinos Island, Cyclades, Greece. Terra Nova 1, 182–187.

Avigad, D., Matthews, A., Evans, B.W., Garfunkel, Z., 1992. Cooling during the exhumation of a blueschist terrane; Sifnos (Cyclades), Greece. Eur. J. Mineral. 4, 619–634.

Baldwin, S.L., 1996. Contrasting $P-T-t$ histories for blueschists from the Western Baja Terrane and the Aegean: effects of synsubduction exhumation and backarc extension. Subduction: Top to Bottom, vol. 96. American Geophysical Union, Geophysical Monograph, pp. 135–141.

Barnicoat, A.C., Cartwright, I., 1995. Focused flow during subduction: oxygen isotope data from high-pressure ophiolites of the western Alps. Earth Planet. Sci. Lett. 132, 53–61.

Barnicoat, A.C., Cartwright, I., 1997. The gabbro-eclogite transformation: an oxygen isotope and petrographic study of west Alpine ophiolites. J. Metamorph. Geol. 15, 93–104.

Barr, H., 1990. Preliminary fluid inclusion studies in a high-grade blueschist terrane. Mineralogical Magazine 54, 159–168.

Bau, M., 1996. Controls on the fractionation of isovalent trace elements in magmatic and aqueous systems: evidence from Y/Ho, Zr/Hf, and lanthanide tetrad effect. Contrib. Mineral. Petrol. 123, 323–333.

Bebout, G.E., Barton, M.D., 1993. Metasomatism during subduction: products and possible paths in the Catalina Schist, California. Chem. Geol. 108, 61–92.

Bonneau, M., 1984. Correlation of the Hellenide nappes in the South-East Aegean and their tectonic reconstruction. In: Dixon, J.E., Robertson, A.H.F. (Eds.), The Geological Evolution of the Eastern Mediterranean. Geological Society Special Publications, vol. 17. Oxford, Blackwell, pp. 517–527.

Bonneau, M., Blake, M.C., Geyssant, J., Kienast, J.R., Lepvrier, C., Maluski, H., Papanikolaou, D., 1980a. Sur la signification des roches métamorphiques (schistes bleus) des Cyclades (Héllenides, Grèce). L'example de l'île de Syros. C. R. Acad. Sci., Ser. D 290, 1463–1466.

Bonneau, M., Geyssant, J., Kienast, J.R., Lepvrier, C., Maluski, H., 1980b. Tectonique et métamorphisme haute pression d'âge éocène dans les Héllenides: l'example de l'île de Syros (Cyclades, Grèce). C. R. Acad. Sci., Ser. D 291, 171–174.

Bröcker, M., 1990a. Die Blauschiefer-Grünschiefer-Assoziation der Insel Tinos (Kykladen, Griechenland) und ihre kontaktmetamorphe Überprägung. Geotekton. Forsch. 74, 1–107.

Bröcker, M., 1990b. Blueschist-to-greenschist transition in metabasites from Tinos Island (Cyclades, Greece): compositional control or fluid infiltration. Lithos 25, 25–39.

Bröcker, M., 1991. Geochemistry of metabasic HP/LT rocks and their greenschist facies and contact metamorphic equivalents, Tinos Island (Cyclades, Greece). Chem. Erde 51, 155–171.

Bröcker, M., Enders, M., 1999. U–Pb zircon geochronology of unusual eclogite-facies rocks from Syros and Tinos (Cyclades, Greece). Geol. Mag. 136 (2), 111–118.

Bröcker, M., Franz, L., 1994. The contact aureole on Tinos (Cyclades, Greece): Part I. Field relationships, petrography and $P-T$ conditions. Chem. Erde 54, 262–280.

Bröcker, M., Franz, L., 1998. Rb–Sr isotope studies on Tinos Island (Cyclades, Greece): additional time constraints for metamorphism, extent of infiltration-controlled overprinting and deformational activity. Geol. Mag. 135 (3), 369–382.

Bröcker, M., Kreuzer, H., Matthews, A., Okrusch, M., 1993. $^{40}Ar/^{39}Ar$ and oxygen isotope studies of polymetamorphism from Tinos Island. Cycladic blueschist belt. J. Metamorph. Geol. 11, 223–240.

Dixon, J.E., 1969. The metamorphic rocks of Syros, Greece. Unpubl. PhD thesis, University of Cambridge.

Dixon, J.E., Ridley, J.R., 1987. Syros. In: Helgeson, H.C. (Ed.), Chemical Transport in Metasomatic Processes. Reidel, Dordrecht, pp. 489–501.

Dürr, S., 1986. Das Attisch-kykladische Kristallin. In: Jacobshagen, V. (Ed.), Geologie von Griechenland. Borntraeger, Berlin, Stuttgart, pp. 116–148.

Dürr, S., Altherr, R., Keller, J., Okrusch, M., Seidel, E., 1978. The Median Aegean Crystalline Belt: Stratigraphy, structure, metamorphism, magmatism. In: Closs, H., Roeder, D.H., Schmidt, K. (Eds.), Alps, Apennines, Hellenides. Schweizerbart, Stuttgart, pp. 455–477, IUGS Report no. 38.

Ellis, D.J., Green, D.H., 1979. An experimental study of the effect of Ca upon garnet–clinopyroxene Fe–Mg exchange equilibria. Contrib. Mineral. Petrol. 71, 13–22.

Evensen, N.M., Hamilton, P.J., O'Nions, R.K., 1978. Rare earth abundances in chondritic meteorites. Geochim. Cosmochim. Acta 42, 1199–1212.

Fraser, G., Ellis, D., Eggins, S., 1997. Zirconium abundance in granulite-facies minerals, with implications for zircon geochronology in high-grade rocks. Geology 25, 607–610.

Giaramita, M.J., Sorensen, S.S., 1994. Primary fluids in low-temperature eclogites: evidence from two subduction complexes (Dominican Republic and California, USA). Contributions to Mineralogy and Petrology 117, 279–292.

Gieré, R., 1990. Hydrothermal mobility of Ti, Zr and REE; examples from the Bergell and Adamello contact aureoles (Italy). Terra Nova 2, 60–67.

Hecht, J., 1984. Geological Map of Greece 1:50 000, Syros Island. Institute of Geology and Mineral Exploration, Athens.

Höpfer, N., Schumacher, J.C., 1997. New field work and interpretations of the sedimentary sequence, the position of the ophiolitic rocks and subsequent deformation on Syros, Cyclades, Greece. Beih. Eur. J. Mineral. 9, 162.

Höpfer, N., Schumacher, J.C., Raith, M., 1994. Reaction paths in the high pressure metamorphic rocks of Syros (Cyclades). Beih. Eur. J. Mineral. 6, 116.

Katzir, Y., Matthews, A., Garfunkel, Z., Schliestedt, M., 1996. The tectono-metamorphic evolution of a dismembered ophiolite (Tinos, Cyclades, Greece). Geol. Mag. 133, 237–254.

Keay, S., 1998. The geological evolution of the Cyclades, Greece: constraints from SHRIMP U–Pb geochronology. Unpubl. PhD thesis, Australian National University, Canberra, 341 pp.

Krogh, T.E., 1973. A low contamination method for hydrothermal decomposition of zircon and extraction of U and Pb for isotopic age determinations. Geochim. Cosmochim. Acta 37, 485–494.

Krogh, E.J., 1988. The garnet–clinopyroxene Fe–Mg geothermometer — a reinterpretation of existing experimental data. Contrib. Mineral. Petrol. 99, 44–48.

Kötz, J., 1989. Zur Geochemie der Metabasite von Syros, Kykladen, Griechenland. Dr. rer. nat. thesis, Universität Köln, 182 pp.

Maluski, H., Bonneau, M., Kienast, J.R., 1987. Dating the metamorphic events in the Cycladic area: $^{39}Ar/^{40}Ar$ data from metamorphic rocks of the island of Syros (Greece). Bull. Soc. Geol. Fr. (8) t III (5), 833–842.

Matthews, A., Schliestedt, M., 1984. Evolution of the blueschist and greenschist facies rocks of Sifnos, Cyclades, Greece. Contrib. Mineral. Petrol. 88, 150–163.

Melidonis, N.G., 1980. The geological structure and mineral deposits of Tinos island (Cyclades, Greece). Geol. Greece 13, 1–80.

Messiga, B., Tribuzio, R., Bottazzi, P., Ottolini, L., 1995. An ion microprobe study on trace element composition of clinopyroxenes from blueschist and eclogitized Fe–Ti-gabbros, Ligurian Alps, northwestern Italy; some petrologic considerations. Geochim. Cosmochim. Acta 59, 59–75.

Mocek, B., 1994. Geochemische Untersuchungen zur Identifizierung der Protolithe der Hochdrucheinheit von Siphnos, Kykladen (Griechenland). Dr. rer. nat. thesis, Universität Hannover, 199 pp.

Nadeau, S., Philippot, P., Pineau, F., 1993. Fluid inclusion and mineral isotopic compositions (H–C–O) in eclogitic rocks as tracers of local fluid migration during high-pressure high-pressure metamorphism. Earth Planet. Sci. Lett. 114, 431–448.

Nelson, B.K., 1996. Fluid flow in subduction zones; evidence from Nd- and Sr-isotope variations in metabasalts of the Franciscan Complex, California. Contrib. Mineral. Petrol. 119, 247–262.

Okrusch, M., Bröcker, M., 1990. Eclogite facies rocks in the Cycladic blueschist belt, Greece: a review. Eur. J. Mineral. 2, 451–478.

Okrusch, M., Seidel, E., Davis, E.N., 1978. The assemblage jadeite–quartz in the glaucophane rocks of Sifnos (Cyclades Archipelago, Greece). Neues Jahrb. Mineral., Abh. 132 (3), 284–308.

Pan, Y., Fleet, M.E., 1996. Rare earth mobility during prograde granulite facies metamorphism: significance of fluorine. Contrib. Mineral. Petrol. 123, 251–262.

Patchett, P.J., Ruiz, J., 1987. Nd isotopic ages of crust formation and metamorphism in the Precambrian of eastern and southern Mexico. Contrib. Mineral. Petrol. 96, 523–528.

Patzak, M., Okrusch, M., Kreuzer, H., 1994. The Akrotiri unit on the island of Tinos, Cyclades, Greece: witness to a lost terrane of Late Cretaceous age. Neues Jahrb. Geol. Palaeontol., Abh. 194, 211–252.

Pearce, J.A., 1983. Role of the sub-continental lithosphere in magma genesis at active continental margins. In: Hawkesworth, C.J., Norry, M.J. (Eds.), Continental Basalts and Mantle Xenoliths. Shiva Publications, Nantwich, pp. 230–249.

Philippot, P., Selverstone, J., 1991. Trace-element-rich brines in eclogitic veins: implications for fluid composition and transport during subduction. Contrib. Mineral. Petrol. 106, 417–430.

Putlitz, B., Matthews, A., Valley, J.W., 2000. Oxygen and hydrogen isotope study of high-pressure metagabbros and metabasalts (Cyclades, Greece): implications for the subduction of oceanic crust. Contrib. Mineral. Petrol. 138, 114–126.

Ridley, J.R., 1984. Evidence of a temperature-dependent blueschist to eclogite transformation in high-pressure metamorphism of metabasic rocks. J. Petrol. 25, 852–870.

Ridley, J.R., Dixon, J., 1984. Reaction pathways during the progressive deformation of a blueschist metabasite: the role of chemical disequilibrium and restricted range equilibrium. J. Metamorph. Geol. 2, 115–128.

Rubin, J.N., Henry, C.D., Price, J.G., 1989. Hydrothermal zircons and zircon overgrowths, Sierra Blanca Peaks, TX. Am. Mineral. 74, 865–869.

Rubin, J.N., Henry, C.D., Price, J.G., 1993. The mobility of zirconium and other “immobile” elements during hydrothermal alteration. Chem. Geol. 110, 29–47.

Scambelluri, M., Rampone, E., 1999. Mg-metasomatism of oceanic gabbros and its control on Ti-clinohumite formation during eclogitization. Contrib. Mineral. Petrol. 135, 1–17.

Scambelluri, M., Piccardo, G., Philippot, P., Robbiano, A., Negretti, L., 1997. High salinity fluid inclusions formed from recycled seawater in deeply subducted Alpine serpentinite. Earth Planet. Sci. Lett. 148, 485–499.

Scambelluri, M., Pennacchioni, G., Philippot, P., 1998. Salt-rich aqueous fluids formed during eclogitization of metabasites in the Alpine continental crust (Austroalpine Mt. Emilius unit, Italian Western Alps). Lithos 43, 151–167.

Schliestedt, M., 1986. Eclogite–blueschist relationships as evidenced by mineral equilibria in the high-pressure rocks of Sifnos (Cycladic islands), Greece. J. Petrol. 27, 1437–1459.

Schliestedt, M., Altherr, R., Matthews, A., 1987. Evolution of the Cycladic crystalline complex: petrology, isotope geochemistry and geochronology. In: Helgeson, H.C. (Ed.), Chemical Transport in Metasomatic Processes. Reidel, Dordrecht, pp. 389–428, NATO ASI Series.

Seck, H.A., Kötz, J., Okrusch, M., Seidel, E., Stosch, H.G., 1996. Geochemistry of a meta-ophiolite suite: an association of meta-gabbros, eclogites and glaucophanites on the island of Syros, Greece. Eur. J. Mineral. 8, 607–623.

Selverstone, J., Franz, G., Thomas, S., Getty, S.R., 1992. Fluid variability in 2 GPa eclogites as an indicator of fluid behaviour during subduction. Contrib. Mineral. Petrol. 112, 341–357.

Sorensen, S.S., Grossman, J.N., 1993. Accessory minerals and subduction zone metasomatism: a geochemical comparison of two mélanges (Washington and California, USA). Chem. Geol. 110, 269–297.

Steiger, R.H., Jäger, E., 1977. Subcommission on geochronology: convention on the use of decay constants in geo- and cosmochronology. Earth Planet. Sci. Lett. 36, 359–362.

Stolz, J., Engi, M., Rickli, M., 1997. Tectonometamorphic evolution of SE Tinos, Cyclades, Greece. Schweiz. Mineral. Petrogr. Mitt. 77, 209–231.

Wijbrans, J.R., McDougall, I., 1986. $^{40}Ar/^{39}Ar$ dating of white micas from an Alpine high-pressure metamorphic belt on Naxos (Greece): resetting of the argon isotopic system. Contrib. Mineral. Petrol. 93, 187–194.

Wijbrans, J.R., McDougall, I., 1988. Metamorphic evolution of the Attic–Cycladic Metamorphic Belt on Naxos (Cyclades, Greece) utilizing $^{40}Ar/^{39}Ar$ age spectrum measurements. J. Metamorph. Geol. 6, 571–594.

Wijbrans, J.R., Schliestedt, M., York, D., 1990. Single grain argon laser probe dating of phengites from the blueschist to greenschist transition on Sifnos (Cyclades, Greece). Contrib. Mineral. Petrol. 104, 582–593.

York, D., 1969. Least squares fitting of a straight line with correlated errors. Earth Planet. Sci. Lett. 5, 320–324.